DESIGN AND FATIGUE STUDY OF INTRAVASCULAR CORONARY STENT USING FINITE ELEMENT ANALYSIS

_____

A Thesis

Presented to

the Faculty of the College of Science & Technology

Morehead State University

_____

In Partial Fulfillment

of the Requirements for the Degree

Master of Science

_____

by

Jared May

March 15, 2012

Accepted by the faculty of the College of Science & Technology, Morehead State University, in partial fulfillment of the requirements for the Master of Science degree.
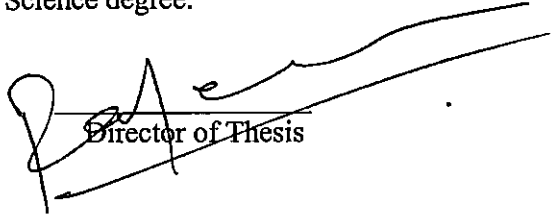
_____
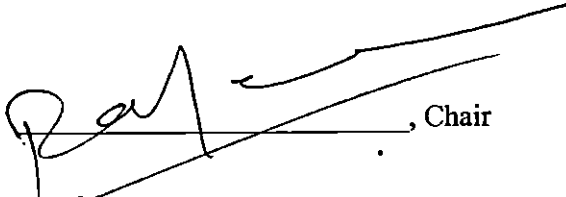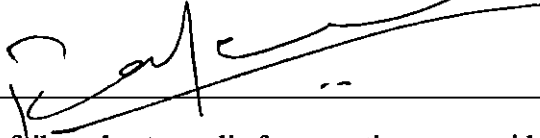Director of Thesis

Master's Committee: _____, Chair

_____

_____
Lloyd R. Jaisingh

_____
Date

DESIGN AND FATIGUE STUDY OF INTRAVASCULAR CORONARY STENTS USING FINITE ELEMENT ANALYSIS

Jared May, M.S.
Morehead State University, 2012

Director of Thesis: _____

Fatigue is a material failure due to cyclic forces acting upon said material. Fatigue can make the material fail before the stresses reach ultimate tensile strength or fracture strength. Intravascular coronary stent are subjected to cyclic loads when placed in vivo. Once in a coronary artery, stents are loaded with systolic and diastolic pulse pressures. The purposes of this research entitled *Design and Fatigue Study of Intravascular Coronary Stents Using Finite Element Analysis* will study the impact of cyclic load on various stent geometries. This research will also parametrically design a coronary stent that will provide comparable fatigue life to commercially available stent designs. SolidWorks design software will be used to create three dimensional geometries of the stents as well as parametrically design a stent. Abaqus finite element analysis software will be used to simulate in vivo artery conditions. It will also be used to crimp the stent models and then deploy them within the artery. The stent fatigue will be analyzed using modified Goodman failure criteria. Each of the stent geometries will be tested using a variety of materials. These materials include 316L stainless steel, nitinol, and poly-L-lactic acid. An analysis of variance will determine if stent geometry, material, or a combination of the two have the greatest impact on fatigue life.

Accepted By: _____, Chair

Lloyd R. Jaisingh

ACKNOWLEDGEMENTS

Table of Contents

List of Figures

List of Tables

Chapter One

Introduction

Disease associated with the buildup of atherosclerotic plaque in the coronary arteries has a high mortality rate in the Western world. The most common of these diseases is coronary artery disease. Coronary artery disease is the deadliest disease in the United States (Lim, 2004). In 2005, a total of 445,687 people died due to complications associated with coronary artery disease (Centers for Disease Control and Prevention, 2010).

Traditionally coronary artery complications are treated using coronary bypass procedures. Bypass procedures are an open surgery in which the chest cavity is opened for the procedure. The heart is also opened during this surgery. The offending artery is removed and replaced with a graft. Coronary bypass procedures are extremely invasive. A surgery of this complicated nature can lead to complications such as infection, immunological graft rejection, etc. Contemporary procedures involve placing an implant known as a stent in the offending artery. A stent acts as a scaffolding structure that holds and compresses the atherosclerotic plaque and reopens the diseased artery. The stenting procedure is considered to be a minimally invasive procedure when compared to the invasive coronary bypass procedure. The stent is placed on a guide wire system that maneuvers the stent through the body. An opening is made in the femoral artery (the artery located along the thigh). The stent system is then guided through the opening

and along the arterial tree to the diseased artery. Stents are currently being manufactured from various materials including metals and polymers. Coronary stenting provides an attractive alternative to coronary bypass. A coronary intervention is needed due to a complication known as stenosis. Stenosis is associated with the closure of an artery due to a buildup of atherosclerotic plaque. However, stenting is not without complications. The risks that generate the most concern are restenosis and stent failure. Restenosis is a vascular phenomenon that is caused by complications due to the stenting procedure. It can lead to an arterial blockage similar to that caused by the initial stenosis. Restenosis can occur for a variety of reasons. Restenosis can occur when the stent imposes a high level of shear stresses on the arterial wall. These shear stresses occur where the stent makes contact with the artery. Shear stress can cause the arterial wall to tear. The body will then attempt to repair the arterial tear by adding layers of smooth muscle tissue to the artery. The smooth muscle tissue can accumulate over time and reclose the artery (i.e. restenosis).

Another concern with coronary stents is mechanical failure. Stents are subjected to cyclic pressures associated with the systolic and diastolic pressures of the heartbeat. Any cyclic load can lead to fatigue in the stent's material. Fatigue can lead to premature material failure in the stent and be a prominent cause in restenosis.

Research Objectives

The objective of this research is to perform a fatigue analysis on various commercially available stent geometries using finite element analysis. The stents will be tested using a combination of various biologically accepted materials. The objective will be to determine the fatigue life of these commercial stent utilizing these biologically accepted materials. The materials tested will include 316L stainless steel, Nitinol, and poly-L-lactic acid. A statistical analysis will be performed to determine if material is a significant determinant in fatigue life.

Limitations

This research will not take drug eluting stents into account. Drug eluting stents are stents that releases small doses of medication such as paclitaxel. Drug eluting stents help to limit the occurrence of a blood clot, or arterial thrombosis. Thrombosis can cause restenosis due to a blood clot that forms and blood flow stagnation around the stent. Therefore, thrombosis is not considered in the research as well.

Hemodynamics will not be considered. Hemodynamics is the study of blood flow through the artery.

The balloon interaction with the stent will not be taken into account. The balloon's interaction with the stent does not significantly contribute to the fatigue life of the stent.

Assumptions

The atherosclerotic plaque will be considered to be symmetrically distributed along the circumference of the artery. The artery will be modeled to represent a concentric plaque.

It will be assumed that the patient whose artery will be modeled has no genetic predisposition to diabetes. Diabetes can change the mechanical properties of the arterial wall. Diabetes can lead to higher circumferential stress in the artery at lower strain rates (Fung, 2002).A genetic predisposition to heart disease can cause an onset of myocardial infarction at an early age. The patient will be considered to have a mean age of 65.9 years (Ellis & Holmes, 2000). This mean age of 65.9 years will allow for the assumption that the atherosclerotic plaque has accumulated naturally overtime leading to the eccentric plaque in the aforementioned assumption.

Significance of the Study

Predicting coronary stent failure is an adequate method for determining the onset of in-stent restenosis. Stents are subjected to cyclic loading once placed *in-vivo*. Cyclic loading can lead to stent fatigue (reducing the stent's radial strength) and material failure. A loss of radial strength can lead to a collapse of the stented artery and thus restrict blood flow.

This study will analyze the fatigue life of a commercially available stent made of different materials. The study will determine the significance of stent material and design when determining fatigue life.

Definition of Terms

- *Adventitia*: the outer most layer of the arterial wall. The adventitia is comprised of collagen fibers (Hastings, 1992).

- *Atherosclerosis*: A physiological phenomena in which the arterial wall thickens, hardens, and eventually loses its elastic properties (Wang, 2001).

- *Coronary Artery*: Arteries that supply oxygen rich blood to the heart muscle.

- *Coronary Artery Disease*: A plaque buildup in the coronary artery. Coronary artery disease is often associated with atherosclerosis.

- *Hyperelastic Material*: A material in which the derivative of the strain density equals the stress per unit volume (Mase, 1970).

- *Intima*: The inner most layer of the arterial wall. The lumen is made of endothelial cells (Hastings, 1992). The intima is contacts the blood in a healthy artery.

- *Lumen*: The passageway in the artery in which blood flows.

- *Media*: The center layer of the arterial wall. The media determines the arteries elastic properties. It is made of collagen and elastin fibers. A high concentration of elastin fibers gives the artery a high elasticity (Hastings, 1992).

- *Myocardium*: Heart muscle.

- *Restenosis*: A decrease in arterial lumen that is usually associated with coronary intervention procedures. Restenosis occurs due to arterial elastic

recoil that can lead to a thickening of the adventitia (Migliavacca, et al., 2004).

- *Shape Memory Alloy*: A material that returns to its original cold worked shape under the influence of thermal or other mechanical stresses.

- *Stenosis*: A reduction of arterial lumen usually due to an atherosclerotic buildup.

Chapter Two

Literature Review

In this chapter, an overview of the human coronary artery will be presented. The formation and types of atherosclerotic plaque will also be presented along with an overview of the stent procedures. The basic finite element method will be described in terms of global stiffness matrices. A background study into stent analysis will also be described.

Artery Overview

The artery is a passageway that transports oxygen rich blood from the myocardium to the rest of the human body. Coronary arteries provide oxygenated blood from the lungs to the myocardium. A restriction in the coronary artery can lead to a decreased blood flow to the myocardium. This blood flow reduction can lead to myocardial infarction, or heart attack. Myocardial infarction occurs when the heart muscle does not receive enough oxygen to properly function. The cells in the myocardium then begin to die due to oxygen starvation.

A healthy artery consists of three layers: the intima, the media, and the adventitia. Figure 1 illustrates the layers of the arterial wall.
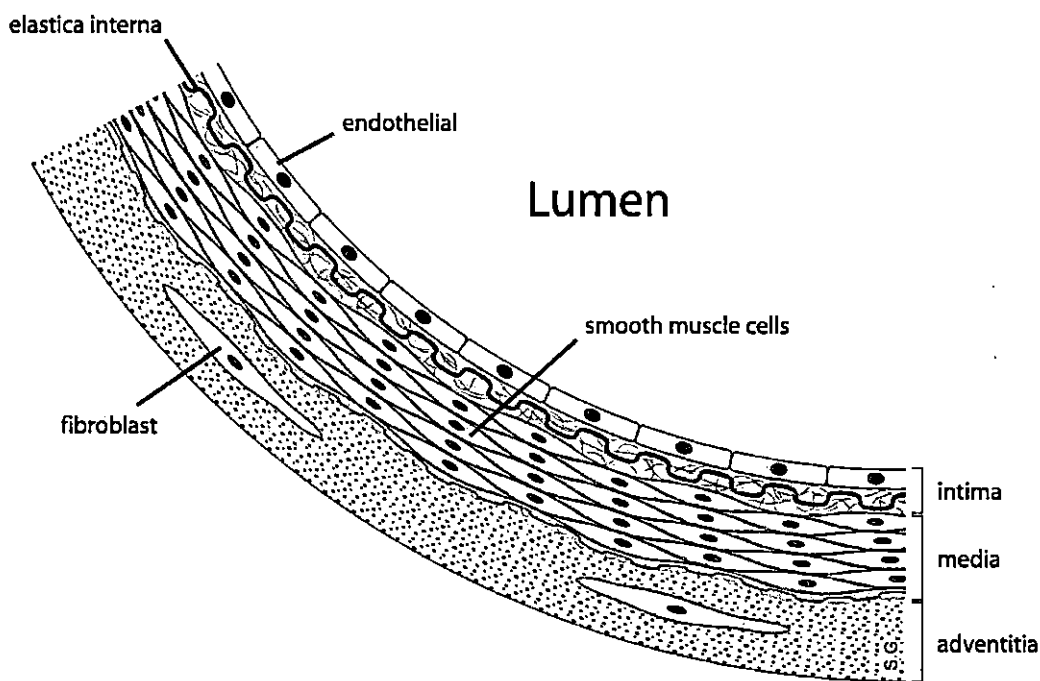
Figure 1. The layered structure of the arterial wall (Mortier, 2010).

The layers of the artery are composed of two major fibers: elastin and collagen. Elastin is a non-linear elastic material. It has an incremental Young's modulus of $3*10^5$ Pa at a strain of 40% (Hastings, 1992). Collagen is a stiffer material possessing a Young's modulus of 10^8 Pa at a strain of 3% to 4% (Hastings, 1992). These two fibers act in tandem to give the artery its elastic and structural properties.

The endothelium is a portion of the intima that contacts the blood. The intima consists of collagen fibers. The intima is the thinnest layer of the artery and does not serve a significant role in the artery's structural integrity.

The media has different compositions throughout the human body. Larger coronary arteries consist of elastin fibers (Hastings, 1992). These elastin fibers give larger arteries a high degree of elasticity. Smaller arteries are made up of smooth muscle as well as a matrix of elastin and collagen. Smaller arteries are less elastic than their larger counterparts.

The adventitia is exclusively made up of collagen fibers. The adventitia is the arteries main structural component of the artery.

Arteries are subjected to pre-tensioning stresses in the body which serve to tether the artery to the surrounding connective heart tissue. This *in-vivo* tethering allows the artery to move in both the radial and longitudinal directions (Hastings, 1992). It is well documented that an artery that is removed from the body will undergo a significant reduction of length (Green, Schajer, Parker, & Post, 1995). The artery length can have a reduction of up to 50% the original length. This reduction indicates an *in-vivo* arterial pre-tensioning. Therefore, an artery removed from the body is said to be in a no-load state. Fung proposed that an artery placed *in-vitro* can be returned to its *in-vivo* state by stretching the artery along its central longitudinal axis (Fung, 2002).

The artery is a complex mechanical structure. The artery does not have a linear stress and strain relationship. Therefore, it is difficult to determine an exact Young's modulus for the artery. An incremental Young's modulus can be calculated using assumptions that the artery is an incompressible and isotropic material. Hasting

provides means for calculating the incremental Young's modulus for an artery based upon assumptions of pseudo-elasticity (Hastings, 1992).

$$E_{inc} = \frac{\Delta P R_o R_i^2 2(1-v^2)}{\Delta R_o (R_o^2 - R_i^2)}$$

(1)

Where:

R_o is the outer artery radius

R_i is the inner artery radius

ΔR_o is the change in outer radius due to a pressure

ΔP is the change in pressure

v is the Poisson's Ratio

A more accurate view of the artery's elastic nature can also be modeled using deformable continuum mechanics theory. The artery does not have a linear stress/strain relationship and can therefore be can be modeled as a hyperelastic solid. A hyperelastic solid can be defined using a strain density function based upon the principles stretches of the material. The basic form of the artery's constitutive equation is shown below (Simulia).

$$U^{def} = C_{ij} \left(I_1 - 3\right)^i \left(I_2 - 3\right)^j + \sum_{i=1}^{N} \frac{1}{D_1} \left(J_{el} - 1\right)^{2i}$$

(2)

Where:

U^{def} is the material strain density function

C_{ij} is a material constant (the subscripts i and j describe the direction)

I_1 is the first Cauchy strain invariant

I_2 is the second Cauchy strain invariant

D_1 is the material compressibility factor

J_{el} is material elastic volume strain

The Cauchy stress invariants are defined in terms of the principle stresses. The first and second Cauchy stress invariants can be defined as follows.

$$I_1 = \lambda_U^2 + 2\lambda_U^{-1} \tag{3}$$

$$I_2 = \lambda_U^{-2} + 2\lambda_U \tag{4}$$

Where:

λ is the principal stretch

Atherosclerosis Formation and Types:

Atherosclerosis formation is a complex biological process that is characterized by a hardening of the artery due to an increased concentration of smooth muscle cells in the intimal artery layer (Raines & Ross, 1995). The increased number of smooth muscle cells causes the intima to thicken.

Normal atherosclerotic growth typically occurs over several decades and can begin in the infant and toddler years. Atherosclerotic plaque begins as an inflammation in the endothelium cells of the intima (Ross, 1999). Fatty streaks form in the arteries during the early stages of life. This fatty streak is associated with an arterial wall inflammation, thus leading to a slight reduction of the lumen. The diseased endothelium gains an adhesive property. Lipids then begin to accumulate around these adhesive fatty streaks as the person ages. The accumulation of lipids

incites an immunological response in the artery. The artery attempts to recover through an accumulation of smooth muscle cells. The smooth muscle cells intertwine with the lipid leading to a complicated atherosclerotic lesion. The artery will then attempt to recover (Ross, 1999). During the arterial recovery process, the artery wall thickens. The thickened arterial wall helps to dilate the lumen and keep constant blood flow. After remodeling, the artery wall will continue to inflame and release various growth factor enzymes (Ross, 1999). This inflammation process leads to necrosis in which the artery cells begin to die. Smooth muscle cells begin to accumulate around the diseased lesion once again. A fibrous cap forms over the lesion and covers the lipid, smooth muscle, and necrotic core. This is known as a complicated lesion. Figure 2 illustrates the atherosclerosis accumulation process.
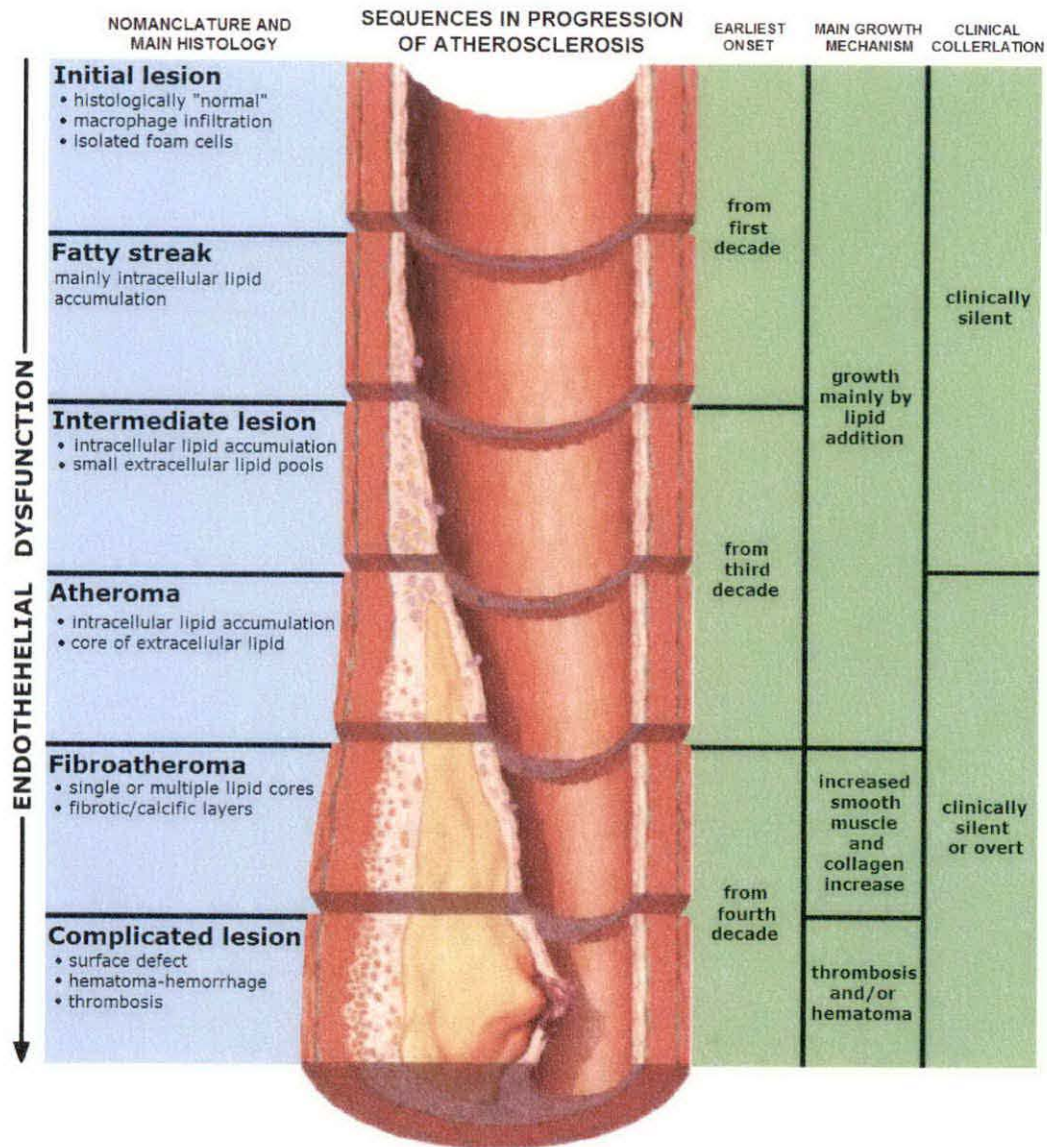
Figure 2. Atherosclerosis growth and complication (Forensic Medicine for Medical Students, 2010).

Myocardial infarction can then occur when the blood flow induced stresses rupture the fibrous cap surrounding the lesion. The rupture leads to a blood clot (also

known as thrombosis). The blood clot reduces the blood flow to the heart, thus starving it of oxygen. This oxygen starvation leads to necrosis of the myocardium.

There are various components of an atherosclerotic plaque. One such component of plaque is the calcified plaque. Calcified atherosclerosis is associated with an aged lesion which tends to possess an increased collagen density similar to the collagen densities found in bone (Fitzpatrick, Edwards, & Ingram, 1994). Calcification typically accumulates in the intima layer of the artery. The calcification leads to intimal thickening and hardening. The arterial calcification process is almost identical to that process found in the formation of bone. Osteopontitn and osteonectin have been found in calcified intima layers (Bobryshev, Lord, & Warren, 1995). Osteopontitn and osteonectin are minerals found in bone formation.

Atherosclerotic plaque also consists of lipids. Lipids consist of crystalline cholesterol, cholesteryl, and phospholipids (Sirol, 2006). The lipid core of the atherosclerotic plaque forms through the accumulation of fatty streaks that are rich with lipid cells (Ross, 1993). Lipid concentration can influence the intensity of the mechanical stresses within the atherosclerotic plaque. A larger lipid core can lead to higher stresses within the plaque and artery (Huang, et al., 2001). The lipid concentration has been known to lead to a structure weakening of the arterial wall (Guyton & Klemp, 1989). These stresses can then lead to plaque rupture and myocardial infarction. The lipid core forms between the fibrous cap and the intimal layer.

A third component of atherosclerotic plaque is a fibrous cap. The fibrous cap is made up of smooth muscle tissue, extracellular material (collagen, proglycans, and elastin fibers) (Sirol, 2006). The fibrous cap covers the vulnerable lipid core and necrotic smooth cells (Bennett, 2007). Plaque rupture can occur if the fibrous cap is thin. The thin fibrous cap acts as a stress concentrator and thus can rupture under relatively low physiological forces.

Stenting Overview

Over one million stenting procedures are performed worldwide each year (Kandzari, Tcheng, & Zidar, 2002). Stents act as a scaffolding structure that compresses the complicated atherosclerotic lesion. Cardiovascular stents are placed and expanded within the offending artery. The stenting procedure is a minimally invasive coronary intervention. The procedure involves placing the stent and deployment balloon on a catheter and guide wire. The stent system is typically placed in the peripheral artery in the thigh. The stent is then guided through the cardiovascular tree to the offending artery. Interventional radiology in the form of x-ray is used to aid the cardiologist in maneuvering the stent. Once the stent is in place, it is expanded within the artery.

Stents are traditionally manufacturer from biologically compliant metals. These metals include 316L stainless steel, cobalt chromium, and tantalum among others. Biocompatibility is extremely important when designing a stent. If the stent material is not biologically compatible, an immunological response can be incited

with the artery. This immunological response can include arterial trauma such as inflammation and scarring (Lim, 2004). Other severe immunological reactions include chronic inflammation and toxin buildup as the immune system attacks the stent. Any immune system response can lead to thrombosis and in-stent restenosis. Another potential problem with stents is the complication of restenosis. Stent design can directly influence restenosis rates. Restenosis is typically associated with the small, less elastic arteries but can still be a significant risk factor in the elastic coronary arteries. Studies have shown that stents with thicker struts (greater than 0.10 mm) can cause higher restenosis rates than those stents with thin struts (Briguori, et al., 2002). Thicker struts can lead to higher stresses in the arterial wall. In-stent restenosis is primarily an inflammatory response. Restenosis involves neointimal hyperplasia or intimal remodeling (Kornowski, et al., 1998). The stent struts have a tendency to cause shear stresses along the contact boundary between the stent and artery. The arterial remodeling involves an accumulation of smooth cells along the site of the shear stresses (Glagov, 1994). These smooth cells can get accumulated to the point that the lumen is once again blocked in spite of the stent; hence the in-stent restenosis phenomenon. Figure 3 demonstrates the basic in-stent restenosis process.
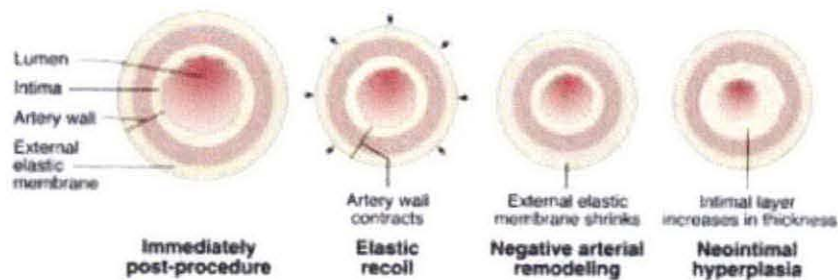
Figure 3. In-stent restenosis stages and formation (Masia, 2008).

Drug eluting stents may be another method besides optimized strut design that can combat the occurrence of in-stent restenosis. Drug eluting stents are coated with antithrombogenic medicines such as paclitaxel or sirolimus (Poerner, Haase, Wiesinger, Wiskirchen, & Duda, 2002). These stents are typically 316L stainless steel or cobalt chromium stent coated with the anti-thrombogenic medication. The medication is released of time to offset the biological agents responsible for in-stent restenosis.

Contemporary stents are beginning to be manufactured from more exotic materials that have promising biocompatibility and structural integrity. One such exotic material is Nitinol, a nickel and titanium alloy. Nitinol exhibits superelastic and shape memory characteristics. The superelastic and shape memory characteristics are enabled through thermo-mechanical response to stresses. These characteristics allow Nitinol to recover its original shape through a process of mechanical unloading (Petrini, Migliavacca, Dubini, & Auricchio, 2003). Nitinol's shape memory properties exist because the metal transforms between an austenitic

composition and a martensitic composition under mechanical loading and exhibits the

stress/strain relationship shown in the figure below.
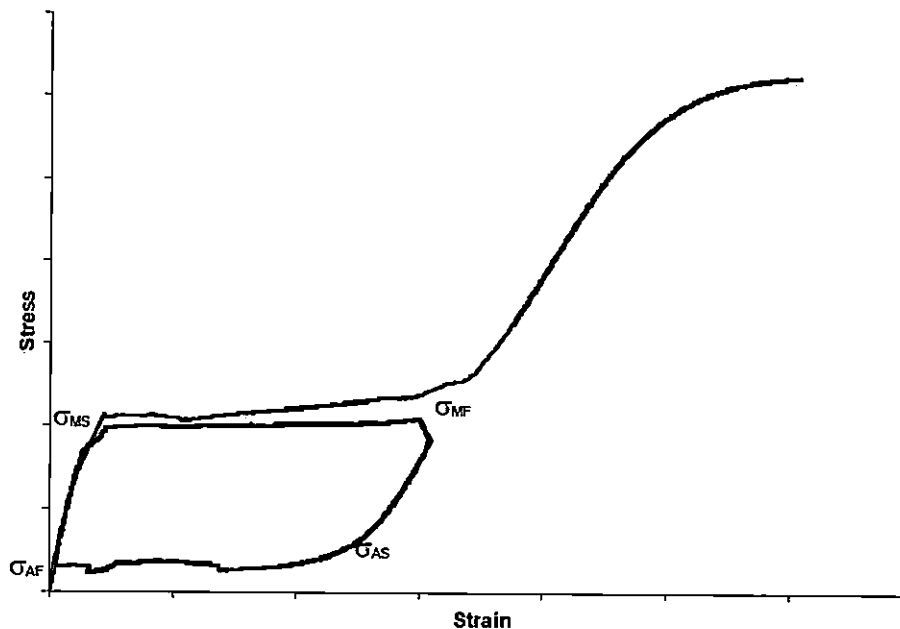
Figure 4. Stress/strain relationship for Nitinol (Gopal, Kim, Swift, & Choules, 2008).

The stress/strain plot in Figure 4 illustrates the three major components of the

Nitinol stress response. The initial phase of the Nitinol stress response is an

austenitic loading. Nitinol then transitions to its martensitic composition at strains of

0.8% (Gopal, Kim, Swift, & Choules, 2008). The stress/strain plot also consists of a

superelastic area in which the Nitinol exists as both austenite and martensite. This

mixture of austenite grain structures and martensite grain structures exists at strains of

0.8% to 6% (Gopal, Kim, Swift, & Choules, 2008). Strains are fully recoverable in

the superelastic region because the ratio of austenite to martensite changes to

compensate for the varying stresses. An elastic-plastic region exists beyond strains of

8% (Gopal, Kim, Swift, & Choules, 2008). This region marks the transition to a full martensitic grain structure and plastic deformation.

Stents are also manufactured using biodegradable polymers. Biodegradable polymer stents are absorbed into the body over a period of time. These biodegradable stents have shown to induce minimal thrombosis, moderate neointimal remodeling, and low rates of inflammation (Masia, 2008). Contemporary biodegradable stents are being manufactured from poly-L-lactic acid (PLLA). Studies in rabbit arteries showed that a PLLA stent had no inflammation response during the first six months (Masia, 2008). The stent was completely degraded and absorbed with 24 months. Biodegradable polymer stents have desirable physiological characteristics but do not possess desirable mechanical properties (like mechanical strength for example) when compared to metallic stents. Therefore, polymer stent must be designed with thicker struts. The thicker struts allow the stent to overcome the compressive radial forces imposed by the artery and the radial forces imposed by systolic and diastolic pulse pressures.

PLLA is the most common biodegradable polymer stent material and exhibits a viscoelastic nature. This viscoelastic state of PLLA introduces internal forces that are created due to a distortion of the polymer chains in response to the external load whenever an external load is applied. The viscoelastic response in PLLA exhibits a stress relaxation, creep, and hysteresis. The stress response of PLLA can be shown by the following equation (Masia, 2008).

$$U = \frac{\rho RT}{2M_W}(\lambda_1^2 + \lambda_2^2 + \lambda_3^2 - 3) \tag{5}$$

Where:

λ is the principle stretch

ρ is the density

R is the universal gas constant

T is the absolute temperature

M_W is the polymer molecular weight

The stress response of PLLA can be further represented through the use of hyperelastic constitutive modeling. A polynomial strain density function can be used to model the hyperelastic response of PLLA.

$$U^{def} = C_{ij}(I_1 - 3)^i (I_2 - 3)^j + \sum_{i=1}^{N} \frac{1}{D_1}(J_{el} - 1)^{2i} \tag{6}$$

Where:

U^{def} is the material strain density function

C_{ij} is a material constant

I_1 is the first Cauchy strain invariant

I_2 is the second Cauchy strain invariant

D_1 is the material compressibility factor

J_{el} is material elastic volume strain

The stent's material determines the stent classification. Stents can be classified as either balloon expanding or self-expanding. Traditional metallic stents

and polymer stents are balloon expandable stents. These stents use a balloon

mounted catheter to expand the crimped stent within the artery. The balloon expands

and applies a constant pressure against the crimped stent. Self-expanding stents are

manufactured from shape memory alloys such as Nitinol. These stents are able to

expand to their pre-crimped diameter by releasing the stored strain energy. Self-

expanding stents are crimped to the catheter. A removable sheath is placed over the

stent and the removed once the stent is located at the offending lesion. The stent

recovers its pre-crimped diameter once the sheath is removed.

Finite Element Analysis

Finite element analysis (FEA) is a branch of the finite element method (FEM)

that enables engineers to solve complex problems. FEA is based upon the theory that

a solid structure is a continuous element or a continuum (Budynas & Nisbett, 2006).

FEA separates this continuous structure into discrete elements. A complex solid

structure can contain thousands of discrete elements to form what is known as a

mesh. Each element of the mesh is connected by exterior nodes (Hutton, 2004).

Boundary conditions are applied to these nodes to create a partial differential

equation. Each node contains six degrees of freedom to which boundary conditions

can be applied. The six degrees of freedom include translation in X, Y, and Z axes

and rotation X, Y, and Z axes. Boundary conditions can include limitations on the

analysis such as limiting nodal displacement and/or rotation. The discrete elements

are also given the mechanical properties of the structure's defining material. The

properties can include elastic and plastic properties.

The basic finite element can be thought of as a spring that can be defined by the

following equation (Budynas & Nisbett, 2006).

$$k = \frac{AE}{l} \tag{7}$$

Where:

k is the spring rate

A is the element cross-sectional area

E is the material's Young's modulus

l is the element length

This spring element consists of nodes positioned at each end for a total of two nodes.

These nodes can be designated as node one and two. The forces in the nodes can be

represented by displacement equations (Budynas & Nisbett, 2006).

$$f_{1,e} = k_e(u_1 - u_2) \tag{8}$$

$$f_{2,e} = k_e(u_2 - u_1) \tag{9}$$

These equations can be combined into a matrix form.

$$\begin{Bmatrix} f_{1,e} \\ f_{2,e} \end{Bmatrix} = \begin{pmatrix} k_e & -k_e \\ -k_e & k_e \end{pmatrix} \begin{Bmatrix} u_1 \\ u_2 \end{Bmatrix} \tag{10}$$

These problems become inherently complex as the number of nodes and

elements in the mesh increase. The complexity of such a problem would be difficult

to solve manually. Finite element analysis software helps aid in solving complex

problems. Finite element software is adept at solving problems that include nonlinear material definitions and large displacements. Therefore, FEA software is capable of calculating the radial displacements of stent subjected to the pulsating pressures of the heartbeat.

FEA software checks complex problems for convergence. The FEA solver routine checks for boundary condition convergence in order to find the solution to stresses and strains present within the problem. Convergence can be checked in two ways. The first method involves increasing the number of degrees of freedom to infinity. This increase is performed by keeping the element size constant. The second method involves decreasing the element size to zero (Tong & Rossettos, 2008).

FEA involves three processes that work to develop the engineering problem. These processes are preprocessing, processing, and post processing. The first process is preprocessing. Preprocessing involves creating the geometric models of the parts to be analyzed. Many FEA software packages allow for the geometry to be imported from computer aided design software. Preprocessing also involves defining material properties for the parts. Meshes of the finite elements are also created during the preprocessing phase. Appropriate forces, boundary conditions, contacts, and part interactions are also defined.

The processing phase of FEA involves submitting the preprocessed analysis to the computer's processor. The partial differential equations are checked for convergence in order to find a solution to the problem.

Post processing occurs after the software has found the solutions. Post processing is necessary in order to view the results from the processor. This phase involves viewing the parts deformed shape as well as relevant stresses and strains.

Background Study

Significant research has gone into the study of arterial wall mechanics and intravascular stent response. Early and Kelly studied the impact of arterial geometry and material properties on stents. The significance of this study was to define the mechanical properties of the intimal, medial, and adventitial layers of the artery wall and found that these layers are isotropic and incompressible. This nature can be defined by a third order Mooney-Rivlin strain energy function. The strain density function developed by Early and Kelly is given below.

$$W = C_{10}\left(I_1 - 3\right) + C_{01}\left(I_2 - 3\right) + C_{20}\left(I_1 - 3\right)^2 + C_{11}\left(I_1 - 3\right)\left(I_2 - 3\right) + C_{30}\left(I_1 - 3\right)^3 \quad (11)$$

Where:

W is the strain energy function

C is a material constant

I_1 is the first Cauchy strain invariant

I_2 is the second strain invariant

Further studies have also been done to investigate the mechanical properties of atherosclerotic plaques. Maher et al. studied the mechanical response of atherosclerotic plaques from fresh carotid arteries (Maher, Creane, Sultan, Hynes, & Lally, 2009). This study was performed on a total of fourteen atherosclerotic plaques

which consisted of calcified, lipid, and fibrous atherosclerotic plaques. The plaques were found to be isotropic, incompressible hyperelastic materials. The data from the study was fit to a second order polynomial hyperelastic strain energy function.

$$W = C_{10}(I_1 - 3) + C_{01}(I_1 - 3) + C_{20}(I_1 - 3)^2 + C_{11}(I_1 - 3)(I_2 - 3) + C_{02}(I_2 - 3)^2 \quad (12)$$

Where:

W is the strain energy function

C is a material constant

I_1 is the first strain invariant

I_2 is the second strain invariant

Several studies have also been done on stent mechanics. Studies have proven that finite element analysis is a viable method for designing stents as well as testing stent mechanics. Zahedmanesh and Lally studied the impact of strut thickness on in-stent restenosis using finite element analysis (Zahedmanesh & Lally, 2009). They created models of a stenosed artery. They also created models of the ACS RX MultiLink stent and an ACS Multilink RX Duet stent that have dissimilar strut thicknesses. The strut thicknesses were 50 nanometers and 140 nanometers, respectively. The stents were deployed within the stenosed artery model. The study showed that stents with thinner struts led to lower stresses within the arterial wall.

De Beule et al. investigated the phenomena of stent dogboning using FEA (De Beule, Van Impe, Verhegghe, Seger, & Verdonck, 2006). The authors modeled a slotted tube stent using 316LN stainless steel in its unexpanded state. This was

necessary in order to model the stent as a balloon expandable stent. A uniformly distributed pressure was applied to the inside surface of the stent in order to simulate the balloon expansion. Dogboning was defined by the following equation.

$$DB = \frac{R_{distal}^{load} - R_{central}^{load}}{R_{distal}^{load}} \qquad (13)$$

Where:

DB is dogboning

R_{distal}^{load} is the radius of the stent at the distal end under load

$R_{central}^{load}$ is the radius of the stent at the center under load

A distal radius that was significantly larger than the radius of the stent's center indicated dogboning. Dogboning occurred when the ends of the stents inflated to a larger diameter than the center. This caused the end of the stent to contact the artery first, leading to an uneven stress on the artery. De Beule et al. also varied the stent geometry to study the occurrence of dogboning. The study found that asymmetric stent geometry reduced dogboning.

Migliavacca et al. also studied the deployment of a stent in a stenosed artery (Migliavacca, Petrini, Auricchio, & Dubini, 2003). A geometric model of an unexpanded stent and a diseased artery were created. Migliavacca et al. used Abaqus® software to study the large displacements and strains associated with stent expansion. The artery was loaded with a pulse pressure of 110 mmHg. The inside surface of the stent was subjected to a pressure of 2 MPa. The study showed that arterial stresses are concentrated at contact points with the stent. Lesser amounts of

stresses were located at non-contact points. The study also showed that stiffer atherosclerotic plaques require a larger stent inflation pressure to reach the same lumen gain as a softer plaque.

Li and Gu used FEA and parametric design theory to optimize the shape of a periodic curved wire stent. The optimization was done to reduce the stent's elastic recoil and foreshortening after expansion within the artery. This optimization study allowed the dimensions of the stent strut to vary in order to achieve the goals of reducing elastic recoil and foreshortening.

Cervera studied the impact of stenting of the behavior of the arterial wall (Cervera, 2006). He modeled the artery as an idealized, hollow cylinder that was stretched by 59% of its length in order to simulate axial tethering. Matlab was used to create parametric stent geometries. The stents were parameterized in order to include the best features from other stent designs and was used to optimize stent strut spacing, axial amplitude, and the stent's curvature radius. The FEA study involved inflating the artery in order to provide luminal dilation. Each stent created through the parametric study were tested in the artery model and analyzed for critical stresses. It was found that stent geometry influences the magnitude of the stresses present in the arterial wall after stenting. The influence of pulse pressure and compression from the artery also led to an increase in stent hoop stresses (Li & Gu, 2005).

Timmins et al. also studied stent artery mechanics. The authors worked to optimize stent performance. The goal was to optimize the stent geometry in order to minimize stent hoop stresses associated with diastolic pressure. A variety of stent

designs were created and studied. The study showed that in order to reduce the circumferential stent stress, strut spacing need to be increased. It was also determined that the stent design not only affects the structure integrity of the stent but also the stress concentration in the artery. This finding indicated that there must be a compromise between stent structural integrity and arterial wall stresses (Timmins, et al., 2007).

Even though quite a bit of research has used FEA to study the mechanics of arteries and stents, relatively little has been done to study the effect of fatigue on a stent. The majority of these studies were performed on peripheral arteries that are subjected to bending and pulmonary arteries that are subjected to respiration. Hsiao et al. studied the impact of kidney motion and respiration on a cobalt-chromium stent (Hsiao, Nikanorov, Prabhu, & Razavi, 2009). The cobalt-chromium stent was studied in order to see if the stent could withstand 4×10^8 cycles. These cycles represented systolic/diastolic cycles as well as respiratory cycles. The stent model was crimped using FEA and expanded to simulate clinical practices. The stent was then subjected to the systolic/diastolic and respiratory cycles. A Goodman failure criterion was used to analyze the fatigue of the stent. Goodman failure criteria can be defined as shown in the equation below.

$$\left(\frac{\sigma_a}{\sigma_e}\right)+\left(\frac{\sigma_m}{\sigma_u}\right)\geq 1 \tag{14}$$

Where:

σ_a is stress amplitude applied to the stent

σ_e is the material endurance limit

σ_m is the mean stress

σ_u is the material ultimate tensile strength

The fatigue safety factors were determined and plotted to determine the ratio of stress amplitude to the material endurance limit. The study showed that there is no significant risk of fatigue failure in kidney deployed cobalt-chromium stents.

Marrey et al. also studied the fatigue of cobalt-chromium stents. The stent was crimped onto a balloon and then deployed into the artery. The artery was modeled as a hyperelastic tube. After the stent was expanded, pressures representing systolic and diastolic pressures were applied to the inside of the artery. The maximum principle stress was analyzed in order to determine the fatigue life. The fatigue factors of safety were calculated in accordance with modified Goodman failure criteria (Marrey, Burgermeister, Grishaber, & Ritchie, 2006).

Gopal et al. studied the fatigue life of Nitinol. A geometric model of a Nitinol stent was created in order to be studied using FEA. A rigid cylinder was used to expand the stent from its unexpanded state. Axial, bending, and torsional loads were applied to the stent. The mean strain and alternating strain were plotted for each load (Gopal, Kim, Swift, & Choules, 2008).

Perry et al. studied stent fatigue using FEA to analyze the cyclic *in-vivo* pressures and their impact on the stent. It was found that the stent diameter changes *in-vivo* due to the cyclic pulse pressures. These changes in stent diameter induce alternating stresses within the artery. The stent was subjected to one complete cyclic

loading. The mean and alternating stress were computed for each finite element integration point. These stresses were plotted and compared to a modified Goodman diagram. This study also indicated FDA recommendations for stent fatigue testing. Stents must have a minimum fatigue life of 10 years at a heart rate of 72.3 beats per minute. This is equivalent to 380,008,800 pulse cycles (Perry, Oktay, & Muskivitch, 2002).

Li et al. examined the viability of FEA as a tool in studying stent fatigue. A balloon expandable stent was modeled. Cobalt-chromium was chosen as the stent material. Tubular cobalt-chromium specimens were tested in order to develop an accurate material model. The stent was crimped to its *in-vivo* delivery diameter. A rigid cylinder was used to expand the stent to its nominal diameter. A radial compressive force was applied to the outside of the stent in order to simulate the compressive forces of the artery wall and acyclic pressure of 0.0133 MPa was applied to the inside of the stent. The mean and alternating stresses of the finite elements were plotted in a modified Goodman plot. A physical stent was also analyzed using fatigue testing equipment. Latex was used to represent the artery. A saline solution was used to simulate physiological conditions. The results of this physical test were compared to the FEA results indicating that FEA is capable of determining stent fatigue (Li, Lu, Xie, & Li, 2010).

Chapter Three

Problem Statement

In-vivo stent fatigue can lead to stent failure. This can failure can lead to in-stent restenosis, thus leading to a loss of patency within the artery. Finite element analysis techniques combine with appropriate failure criteria can be used to accurately predict stent failure. This research aims to use finite element analysis and modified Goodman failure criteria to analyze the impact of stent design and stent material on fatigue life.

Methodology:

Three dimensional models of stents from Nitinol Devices and Components® (Laserage®) and Cordis® will be created using SolidWorks® design software. A custom design will also be created and optimized using SolidWorks®. SolidWorks® allows user to perform an optimization design study in which variables, constraints, and goals are defined. The variables are the dimensions that are allowed to change within the model. The variables will include stent strut thickness, strut width, and strut length. The constraints for optimization will include the overall length and diameter. It will be necessary for the stent diameter and length to be constrained in order to design a stent that will be compared to commercial stent sizes. The optimization will have several objectives. SolidWorks® Simulation will be used to perform a static stress test on the generated stent designs. The goal will be to

minimize the stress in the stent. The stent strut thickness will also be minimized in order to reduce the chance of in-stent restenosis.

A three dimensional model of an artery and its stenotic plaque will also be created. The artery and plaque will be modeled to represent the *in-vivo* physiological state. This will involve using the FORTRAN programming language to develop an Abaqus® subroutine that will model the artery's hyperelastic behavior. The specific subroutine will be an Abaqus® Standard uhyper routine. The uhyper routine allows for Abaqus® to use complex compressible and incompressible hyperelastic material models. This uhyper routine requires that partial derivatives of the hyperelastic strain energy function be defines with respect to the strain invariants (Simulia). The subroutine will be tested using two dimensional arterial cross sections.

The artery will be modeled in its *in-vitro* phase. Once an artery is removed from the body, it elastically recoils. This recoil indicates that a stent removed from the body is in a no load stated and an artery that is *in-vivo* is in a loaded state (Fung, 2002). The no load model of the stent will be axially stretched in order to simulated the artery's *in-vivo* conditions.

The stent models will be crimped using the Abaqus® adjustable rigid torus extension (Simulia Central, 2011). The adjustable rigid torus extension is an Abaqus® addin specifically designed to model the crimping and expansion of stents. The extension uses a rigid cylinder with a changing radius. The stents will be crimped to allow for a low profile and thus allow the stent to be placed in the stenosed artery model.

A sinusoidal pressure curve will be used to represent the periodic nature of the systolic and diastolic blood pressures. The pressure will be applied to the inside surface of the stent. The alternating stresses will be calculated to determine the stent fatigue life.

An analysis of variance (ANOVA) will be performed to determine if stent design or material is the determining factor in stent fatigue life. Each stent design will be test using 316L stainless steel, Nitinol, and PLLA as the material. Minitab will be used to develop a factorial experimental design to analyze the levels and factors. This experimental design will consist of two factors. The factors will be stent design and stent material, respectively. The stent design factor will have levels of the Nitinol Devices and Components® stent design, the Cordis® stent design, and the custom design. The material factor will have levels of 316L stainless steel, Nitinol, and PLLA. The levels and factors will be measured for its response to fatigue safety factor and fatigue life.

Chapter Four

Chapter four presents the analysis and finding of this thesis. The development and testing of an artery and atherosclerosis are presented using hyperelastic mechanics and finite element analysis. Commercial stent geometries are also presented. The steps necessary to parametrically design a stent are also presented in chapter four. The stent materials properties are defined as well. The stent crimping, expansion, and fatigue mechanics are also presented. A factorial design and its resulting analysis are described at the end of chapter four.

Artery and Atherosclerosis Mechanics and Modeling

Early and Kelly found that the arterial layers (intima, media, and adventitia) can be modeled as an isotropic material (Early & Kelly, 2010). Furthermore, Early and Kelly found that each respective layer exhibits an incompressible hyperelastic nature. Maher et al. also found that fibrous, calcified, and lipid plaques can be modeled using an incompressible hyperelastic strain energy function (Maher, Creane, Sultan, Hynes, & Lally, 2009). The general form of the polynomial hyperelastic strain energy function is shown below (Simulia).

$$U^{def} = C_{ij}\left(I_1 - 3\right)^i \left(I_2 - 3\right)^j + \sum_{i=1}^{N} \frac{1}{D_1}\left(J_{el} - 1\right)^{2i} \tag{15}$$

Where:

U^{def} is the strain energy function

C_{ij} is a material constant

I_1 is the first Cauchy stress invariant

I_2 is the second Cauchy stress invariant

D_1 is the material compressibility factor

J_{el} is the elastic volume strain or third Cauchy invariant

The Cauchy invariants are defined using principle material stretches.

$$I_1 = \lambda_u^2 + 2\lambda_u^{-1} \tag{16}$$

$$I_2 = \lambda_u^{-2} + 2\lambda_u \tag{17}$$

Where:

λ_u is the material principle stretch

An incompressible hyperelastic material has a D_1 value that is equal to zero. This corresponds to a Poisson's ratio of 0.5. The Poisson's ratio can be defined as shown in the following equation.

$$\nu = \frac{3\dfrac{K_o}{\mu_o} - 2}{6\dfrac{K_o}{\mu_o} + 2} \tag{18}$$

Where:

ν is the Poisson's ratio

K_o is the bulk modulus

μ_o is the shear modulus

The incompressibility is further defined using the third Cauchy invariant, J_{el}. The third invariant is equal to one in an incompressible hyperelastic solid. The deformation gradient thus becomes:

$$g = \sum_{i=1}^{N} \frac{1}{D_1}(J_{el} - 1)^{2i} = \sum_{i=1}^{1} \frac{1}{0}(1-1)^2 = \infty \qquad (19)$$

The infinite deformation gradient leads to a solid that does not change volume when undergoing strain.

The incompressibility of a hyperelastic solid can also be described using the principle stretches. Lai et al. showed that an incompressible solid has an equilibrium state shown below (Lai, Rubin, & Krempl, 2010).

$$x_1 = \lambda_1 x_1 \qquad (20)$$

$$x_2 = \lambda_2 x_2 \qquad (21)$$

$$x_3 = \lambda_2 x_3 \qquad (22)$$

Where:

x is the longitudinal direction

λ is the principle stretch in the longitudinal direction

An incompressible solid possesses an equilibrium state between the first and second principle stretches.

$$\lambda_1 \lambda_2^2 = 1 \qquad (23)$$

This equilibrium state leads to an isochoric response in the material (Lai, Rubin, & Krempl, 2010). The isochoric response indicates no change in the material's volume during stretch.

Early and Kelly defined the artery layers using a third order Mooney-Rivlin hyperelastic function (Early & Kelly, 2010). The Mooney-Rivlin strain energy function is a special case of the polynomial strain energy function. The Mooney-Rivlin strain energy function is defined below.

$$U = C_{10}(I_1 - 3) + C_{01}(I_2 - 3) + C_{20}(I_1 - 3)^2 + C_{11}(I_1 - 3)(I_2 - 3) + C_{30}(I_1 - 3)^3 + \frac{1}{D_1}(J_{el} - 1)^2 \tag{24}$$

Table 1 shows the material constant values in megapascals (MPa).

Table 1

Artery Layer Hyperelastic Constants (MPa) (Early & Kelly, 2010)

	C_{10}	C_{01}	C_{20}	C_{11}	C_{30}
Intima	0.08423	0.00505	1.5	0.76506	0.04238
Media	0.00355	0.00066	0.02154	0.01868	0.01977
Adventitia	0.00714	0.00063	0.00803	0.09579	0.09931

Maher et al. defined the atherosclerotic plaque using a second order polynomial strain energy function (Maher, Creane, Sultan, Hynes, & Lally, 2009).

$$U = C_{10}(I_1 - 3) + C_{01}(I_2 - 3) + C_{20}(I_1 - 3)^2 + C_{11}(I_1 - 3)(I_2 - 3) + C_{30}(I_2 - 3)^2 + \frac{1}{D_1}(J_{el} - 1)^2 \tag{25}$$

Table 2 contains the material constants for three varieties of atherosclerotic plaque in MPa.

Table 2

Atherosclerotic Plaque Hyperelastic Constants (MPa) (Maher, Creane, Sultan, Hynes, & Lally, 2009)

	C_{10}	C_{01}	C_{20}	C_{11}	C_{30}
Fibrous	0.00753	0.00999	0.02063	0.00039	0.00078
Lipid	0.00116	0.01168	0.00858	0.0006	0.00022
Calcified	0.001144	0.01357	0.06238	0.02626	0.00761

A FORTRAN subroutine had to be written in order to implement the aforementioned strain energy functions in Abaqus®. In particular, a uhyper routine was written to model the hyperelastic nature of the artery and plaque. The Abaqus® manuals recommend that incompressible materials be modeled as nearly incompressible (Simulia). A bulk modulus to shear modulus ratio of 10,000 was used to model a nearly compressible behavior. A bulk to shear modulus ratio of 10,000 leads to a Poisson ratio of 0.4995. A fully incompressible hyperelastic solid has a Poisson ratio of 0.5. Therefore, a Poisson ratio of 0.49995 has some compressibility.

$$\frac{K_o}{\mu_o} \approx 10,000 \tag{26}$$

$$v = \frac{3\frac{K_o}{\mu_o} - 2}{6\frac{K_o}{\mu_o} + 2} \approx 0.49995 \tag{27}$$

A bulk modulus to shear modulus ratio of 10,000 led to an approximate Poisson's ratio of 0.49995. Therefore, the material compressibility factor (D_1) became non zero. The compressibility factor for each arterial layer and

atherosclerotic plaque were recalculated to obtain a nearly incompressible

hyperelastic response. The compressibility factor is a function of the material's

Poisson's ratio and the linear components of the strain energy function (C_{10} and C_{01}).

$$D_1 = (1-2v)(C_{10} + C_{01}) \tag{28}$$

Table 3 shows the D_I values for each artery layer and plaque component.

Table 3

Hyperelastic Compressibility Factors (MPa)

Component	D_I Value
Intima	0.000008928
Media	0.000000421
Adventitia	0.00000077
Calcified	0.0000014714
Lipid	0.000001284
Fibrous	0.000001752

The uhyper subroutine also required that partial derivatives with respect to the

strain invariants (I_1, I_2, and J_{el}) be calculated. The partial derivatives defined the

elastic response of the strain energy function. These partial derivatives are $\frac{\delta U}{\delta I_1}$, $\frac{\delta U}{\delta I_2}$,

$\frac{\delta U}{\delta J}$, $\frac{\delta^2 U}{\delta I_1^2}$, $\frac{\delta^2 U}{\delta I_2^2}$, $\frac{\delta^2 U}{\delta J^2}$, $\frac{\delta^2 U}{\delta I_1 \delta I_2}$, $\frac{\delta^2 U}{\delta I_1 \delta J}$, $\frac{\delta^2 U}{\delta I_2 \delta J}$, $\frac{\delta^3 U}{\delta I_1^2 \delta J}$, $\frac{\delta^3 U}{\delta I_2^2 \delta J}$, $\frac{\delta^3 U}{\delta I_1 \delta I_2 \delta J}$, $\frac{\delta^3 U}{\delta I_1 \delta J^2}$, $\frac{\delta^3 U}{\delta I_2 \delta J^2}$, and $\frac{\delta^3 U}{\delta J^3}$. These

are the partial derivatives for the artery's Mooney-Rivlin strain energy function. The

uhyper subroutine ignores any partial derivative that is equal to zero. Therefore, these partial derivatives are ignored in the following calculations.

$$\frac{\delta U}{\delta I_1} = C_{10} + C_{11}(I_2 - 3) + C_{20}(2I_1 - 6) + 3C_{30}(I_1 - 3)^2 \tag{29}$$

$$\frac{\delta U}{\delta I_2} = C_{01} + C_{11}(I_1 - 3) \tag{30}$$

$$\frac{\delta U}{\delta J} = \frac{2J - 2}{D_1} \tag{31}$$

$$\frac{\delta U}{\delta I_1^2} = 2C_{20} + 3C_{30}(2I_1 - 6) \tag{32}$$

$$\frac{\delta^2 U}{\delta J^2} = \frac{2}{D_1} \tag{33}$$

$$\frac{\delta^2 U}{\delta I_1 \delta I_2} = C_{11} \tag{34}$$

The partial derivatives for the plaque components were calculated. The plaque components were modeled using a second order polynomial hyperelastic strain energy function.

$$\frac{\delta U}{\delta I_2} = C_{10} + C_{11}(I_2 - 3) + C_{20}(2I_1 - 6) \tag{35}$$

$$\frac{\delta U}{\delta I_2} = C_{10} + C_{11}(I_1 - 3) + C_{30}(2I_2 - 6) \tag{36}$$

$$\frac{\delta U}{\delta J} = \frac{2J - 2}{D_1} \tag{37}$$

$$\frac{\delta^2 U}{\delta I_1^2} = 2C_{20} \qquad (38)$$

$$\frac{\delta^2 U}{\delta I_2^2} = 2C_{30} \qquad (39)$$

$$\frac{\delta^2 U}{\delta J^2} = \frac{2}{D_1} \qquad (40)$$

$$\frac{\delta^2 U}{\delta I_2 \delta_2} = C_{11} \qquad (41)$$

These calculations were compiled into a FORTRAN subroutine. The subroutine was tested using a combination of two dimensional and three dimensional artery models. A two dimensional quarter model was first created in order to test the subroutine and boundary condition assumptions. The artery was modeled in relation to the left anterior descending artery (LAD). Suter et al. prescribed artery layer thickness to lumen diameter ratios (Suter, et al., 2009). The LAD was modeled using the mean lumen diameter of 4.38 mm. The artery was also modeled using the mean outer diameter of 5.45 mm. Holzapfel et al. investigated the ratio of artery layer thickness to artery wall thickness (Holzapfel, Sommer, Gasser, & Regitnig, Determination of Layer-Specific Mechanical Properties of Human Coronary Arteries with Nonatherosclerotic Intimal Thickening and Related Constitutive Modeling, 2005). It was found that ratios for the adventitia, media, and intima were 0.4, 0.36, and 0.27 respectively. These ratios were used to model the artery layer thicknesses.

A two dimensional quarter model of the diseased artery was created by adding a calcified intima, lipid core, and fibrous cap. Figure 5 illustrates the quarter model.
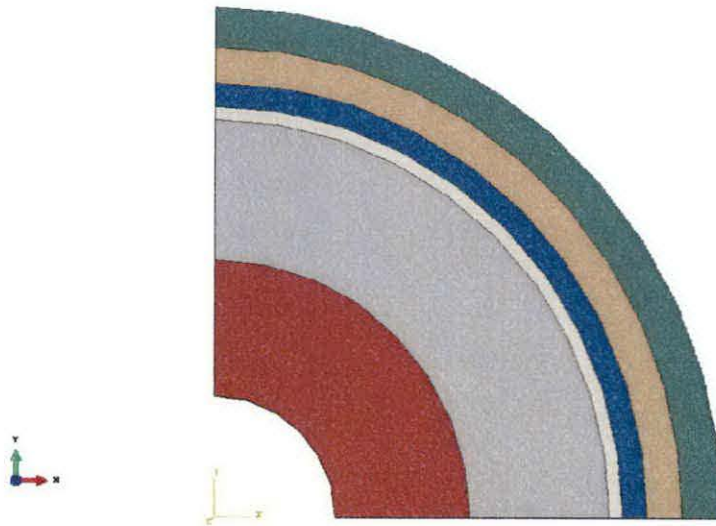
Figure 5. Artery quarter model (green is adventitia; brown is media; blue is intima; white is calcified; grey is lipid core; red is fibrous cap).

The model was meshed using a global seed factor of 0.05. The mesh used CPS4 shell elements. A boundary condition of U_2 equals zero was applied to the nodes along the x axis. Boundary conditions of U_1 equals zero were applied to nodes along the y axis. A boundary condition on degree of freedom U_1 is synonymous with the X axis while U_2 is synonymous with the Y axis. A pressure of 0.013 MPa was applied to the lumen surface of the model. This pressure corresponded to the mean blood pressure through the artery. Figure 6 shows the mesh and boundary conditions.
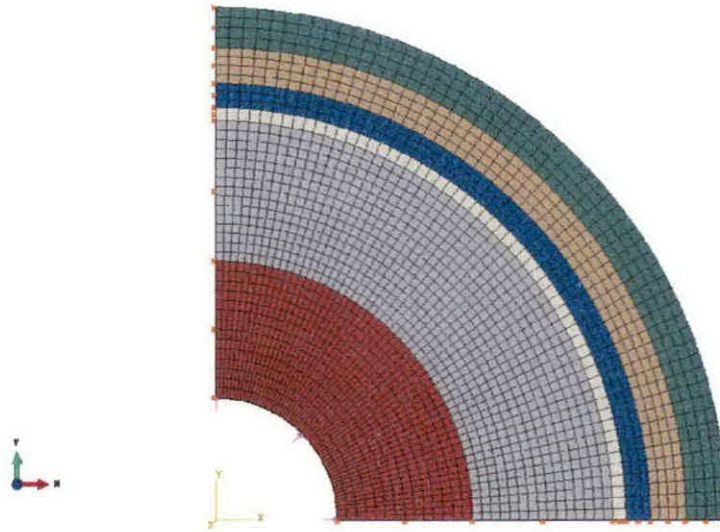
Figure 6. Quarter model mesh and boundary conditions.

The stresses induced by the mean blood pressure is shown is Figure 7.
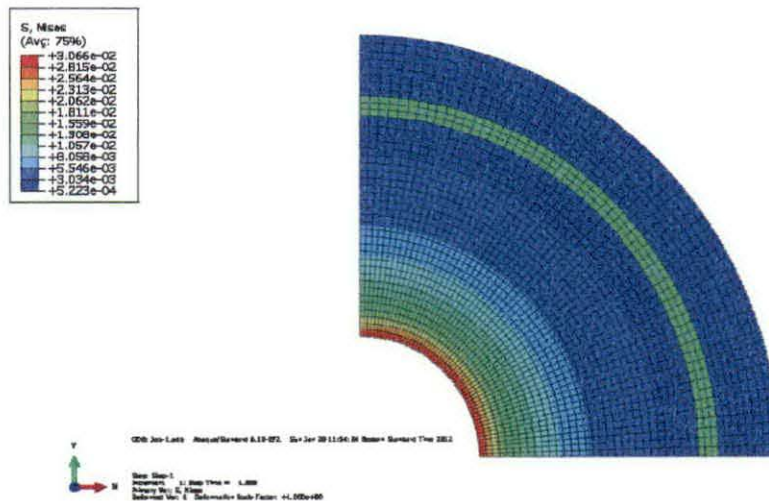
Figure 7. Quarter model von Mises stresses (MPa).

The quarter model was also extended to a two dimensional full model. The same meshing and boundary conditions were applied to the full model. Figures 8 and 9 shows the boundary conditions and stresses.
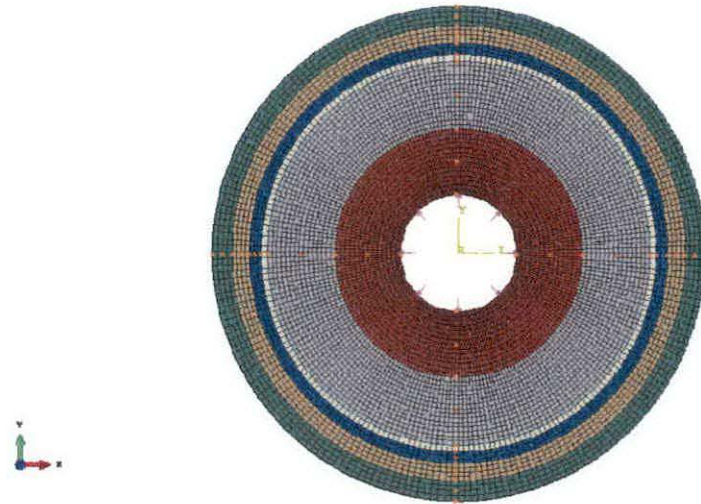
Figure 8. Full model mesh.
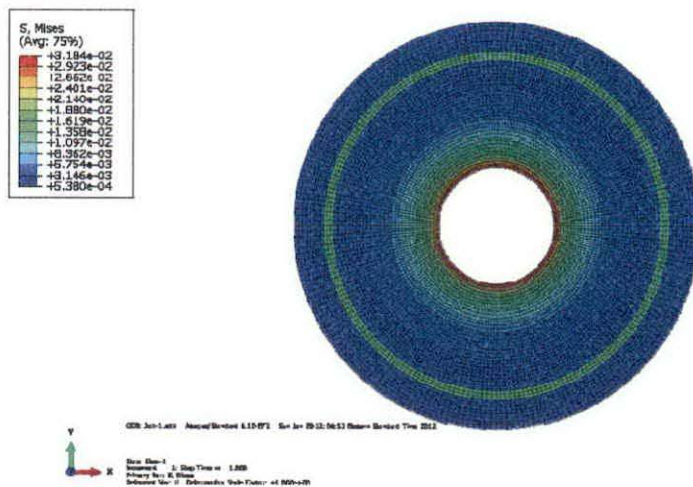
Figure 9. Full model von Mises stresses (MPa).

It is well known that an *in-vivo* artery is in a loaded stated (Fung, 2002). A healthy artery can be stretched up to 50% of its original *in-vitro* length. This *in-vivo* tethering allows the artery to evenly distribute the blood pressure along the endothelium. Fox et al. showed that the LAD can have a length of 32 mm (Fox,

Davies, & Webb-Peploe, 1973). Therefore, an *in-vivo* LAD is stretched by 50%; adding a 16 mm to the total length.

A three dimensional model of the LAD was created using the in vitro length of 32 mm. Displacement boundary conditions of 8 mm were applied in the axial direction. These boundary conditions were applied on both the proximal and distal faces of the artery. Symmetry boundary conditions were also applied to the nodes along the x axis and y axis. Hybrid mesh elements were used to mesh the artery. Hybrid elements enforce a Poisson's ratio of 0.5 in the stiffness matrix. This helped to model the incompressible nature of the arterial wall layers. C3D8H eight node solid brick elements were used to capture the stresses induced by arterial tethering. Figure 10 shows the three dimensional model with the prescribed boundary conditions.

Figure 10. Arterial tethering mesh and boundary conditions.

Von Mises stresses and nodal displacement was monitor to determine the residual state of the *in-vivo* artery. Figure 11 shows the Von Mises stresses and figure 12 nodal displacements.

Figure 11. *In-vivo* arterial layer residual stresses (MPa).
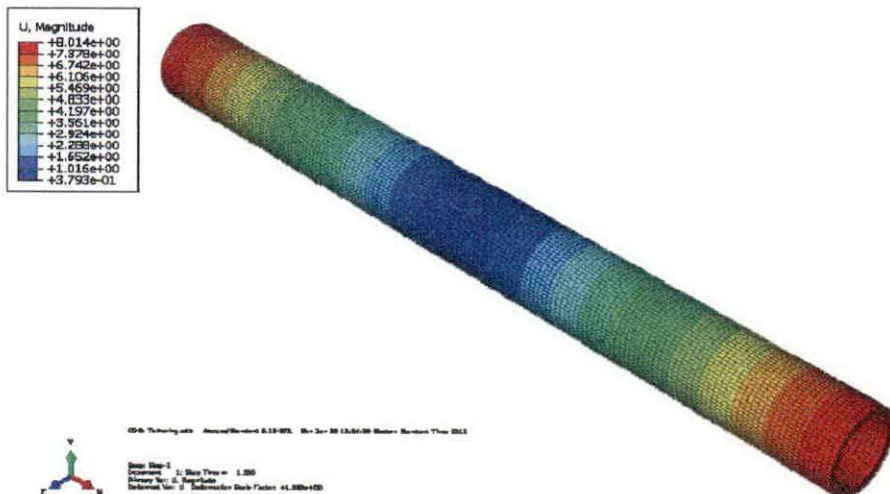
Figure 12. Tethered artery displacement.

Stress was contained within the load bearing adventitia and media layers. The thin intimal layer also had stress concentration. The nodes on the front and back

faces of the artery were displaced using a displacement boundary condition in the X direction. The nodes on the front face were displaced 8 mm and the nodes on the back face were displaced negative 8 mm.

A mean pressure of 0.013 MPa was applied to the tethered artery model. The boundary and mesh conditions from the tethering model were obtained in order to model the *in-vivo* state. Figure 13 illustrates the blood pressure induced stresses.

Figure 13. Arterial stresses due to blood pressure (MPa).
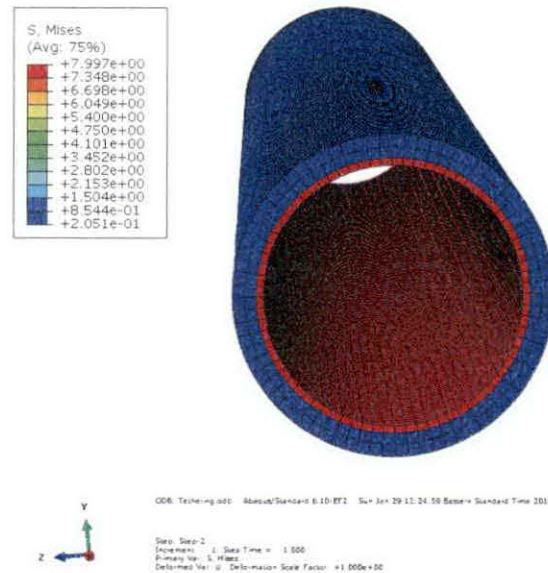
Figure 14. Stresses along the arterial lumen due to blood pressure.

The blood pressure induced a localized stress within the intimal layer. As it is known, the intima serves to isolate the blood from the media and adventitia. The artery model showed the axial load bearing nature of the adventitia and media. It also indicated the blood pressure regulating nature of the intima.

Stent Modeling

SolidWorks® was used to create three dimensional models of the stent geometries. The stents were selected to fit a large coronary artery having a diameter of 4 mm. *The Handbook of Coronary Stents* was surveyed in order to find appropriately dimensioned stents (Rensing, 2007). A slotted tube stent similar to the original Palmaz stent was selected. This stent geometry will be further referred to as stent A in this paper. Stent A was modeled to have an expanded diameter of 4.1 mm and a wall thickness of 0.0635 mm.

A generic test stent from Laserage/Nitinol Devices and components was also selected. This stent will be further referred to as stent B. Stent B was modeled to an expanded diameter of 4.07 mm and a wall thickness of 0.3556 mm. A physical specimen of stent B was available. A photograph of stent B is shown below.

2 mm
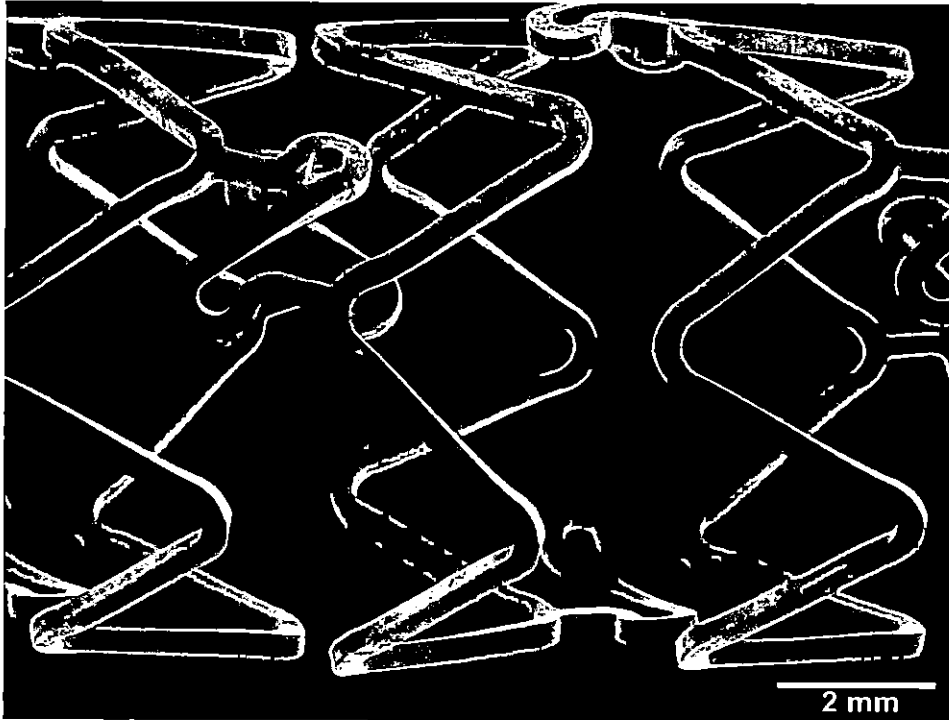
Figure 15. Scanning electron microscope photograph of stent b.

HV	WD	spot	mode	mag 모	pressure	————————— 1 mm —————————
20.00 kV	10.5 mm	3.0	SE	50 x	5.45e-3 Pa	
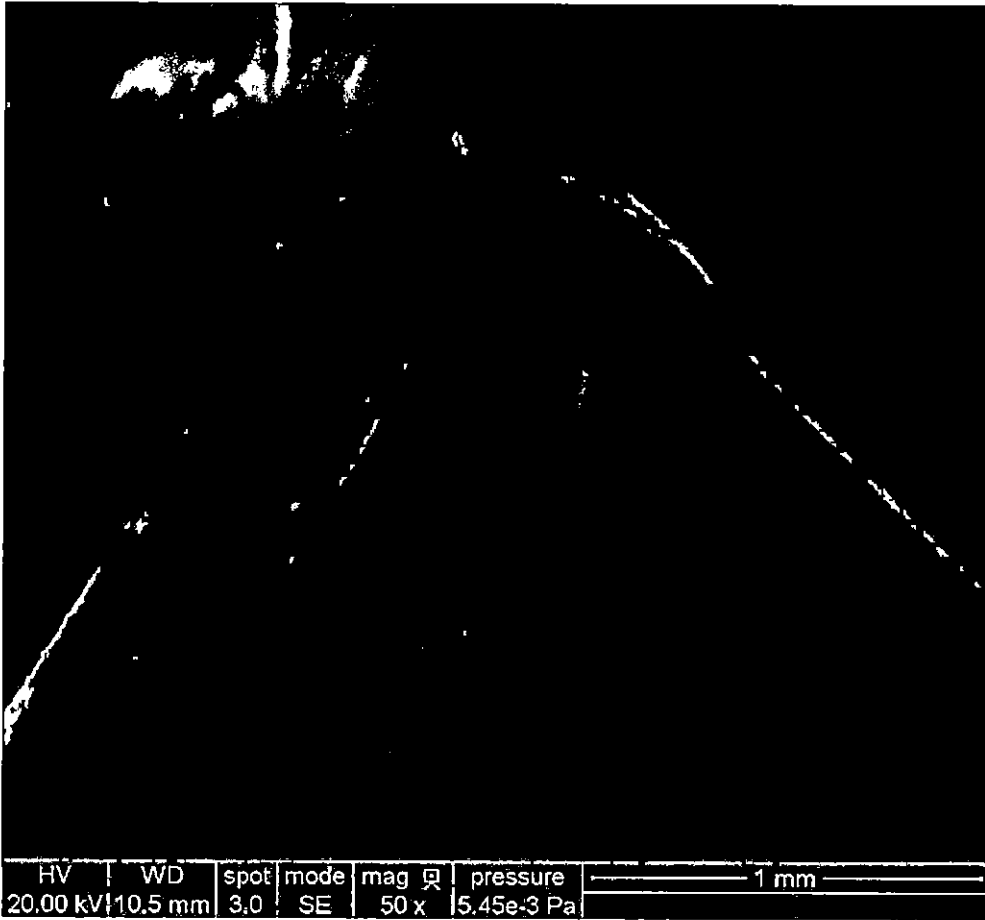
Figure 16. Scanning electron microscope photograph of stent b strut design.

HV	WD	spot	mode	mag 🔍	pressure	——————— 1 mm ———————
20.00 kV	10.0 mm	3.0	SE	50 x	1.55e-3 Pa	
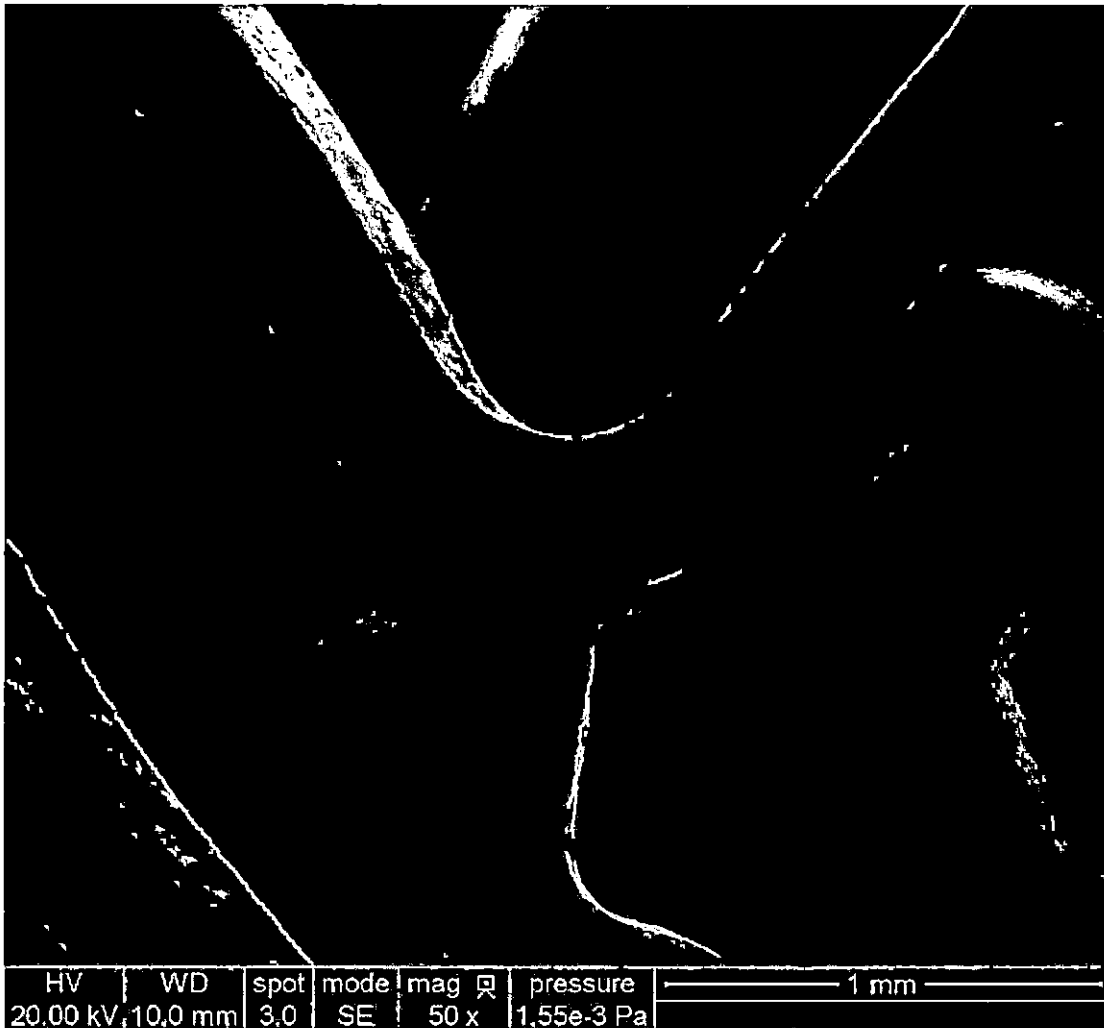
Figure 17. Scanning electron microscope photograph of stent b strut and bridge

connection.

Two rows and bridges of each stent were modeled for symmetry. The use of

symmetry allowed for a better mesh quality and reduction of equations in later steps.

Figure 18 shows the final geometries of stent A and stent B.

(a)   (b)
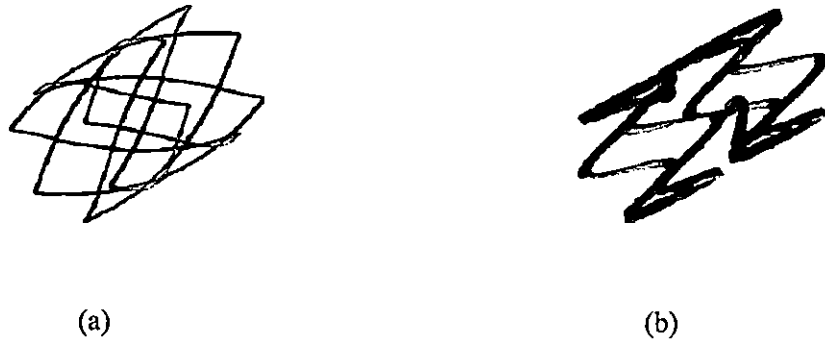
Figure 18. (a) stent a geometry, (b) stent b geometry.

A SolidWorks® design study was performed to design a stent strut geometry

that is capable of minimizing the stresses present within the stent. Bonsignore

showed that a stent strut and bridge configuration can be separated into a series of

beams. The loads on these beams can then be solved to determine the forces and

strains in the stent (Bonsignore, 2010). These forces and strains can be solved using

simple mechanics.

$$\varepsilon = \frac{3w}{L^2}\delta \tag{42}$$

$$F = \frac{12EI}{L^3}\delta \tag{43}$$

Where:

ε is the strain

w is the strut width

L is the strut length

F is the force

E is the material's modulus of elasticity

I is the moment of inertia of the strut cross section

δ is the beam deflection

The Handbook of Coronary Stents shows that the majority of contemporary stents are open cell designs that feature periodic strut patterns (Rensing, 2007). Open cell stents have a lower number of strut connecting bridges as opposed to a closed cell design. Not all adjacent struts are connected to one another in an open cell design. A stent with an open design has more flexibility while providing sufficient radial strength.

A combination of SolidWorks® design studies and SolidWorks® Simulation finite element analysis was used to determine the stresses within the stent. The strut was sketched to a rough approximation of the desired shape. Dimensional variables and constraints were added to the sketch in order to create a parametric study.

The sketch was given a starting thickness of 0.125 mm. An initial FEA study was performed to determine the adequacy of the starting strut design. The stent was meshed using the fine mesh property in SolidWorks® Simulation. A uniformly distributed pressure of 0.016 mm (equivalent to systolic pressure) was applied to the top surface of the strut. Fixed boundary conditions were also applied to one end of the strut as prescribed by Bonsignore (Bonsignore, 2010). Figure 19 shows the mesh along with loading and boundary conditions. The green arrows represent the constrained degrees of freedom due to boundary conditions. The orange arrows represent the location and direction of the uniformly distributed pressure.
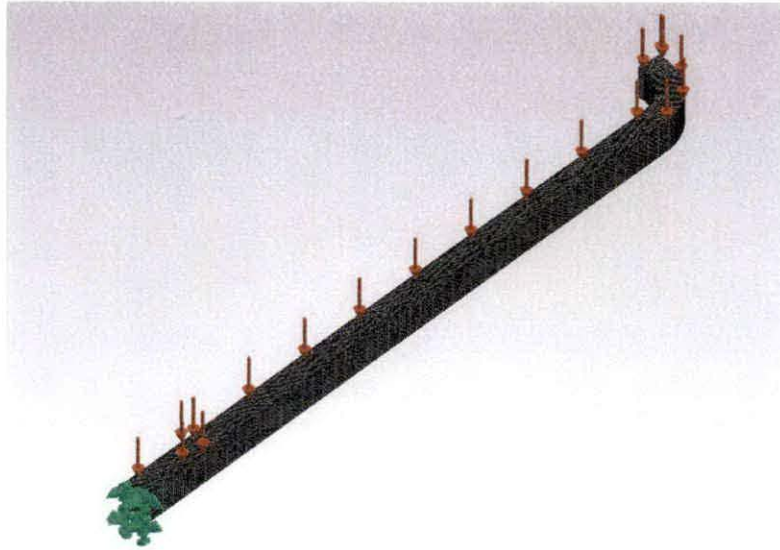
Figure 19. Stent strut loading and boundary conditions.

The strut was found to have a maximum stress of 43.7 MPa as shown

in Figure 20.
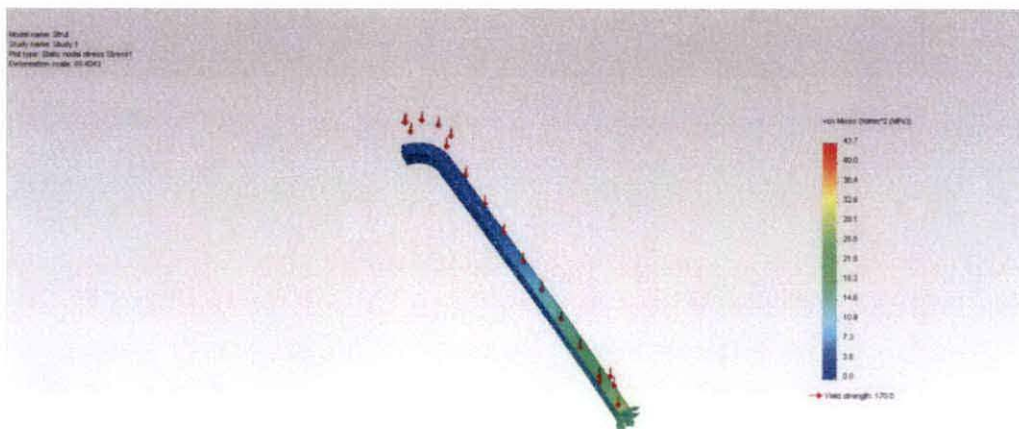
Figure 20. Initial stent strut stresses.

The dimensions were then allowed to change in order to minimize the

maximum stresses present within the strut. The strut half width was allowed to vary

between 0.5 mm and 1.25 mm. Any dimension within this range takes stent crimping

spacing into consideration. The strut length varied from 2.25 mm to 3.25 mm. These

bounds were placed on the strut length in order to keep the strut dimensions at a

reasonable size. Too large a strut length could potentially influence the strut spacing.

The fillet radius was allowed to vary between 0.2 mm and 0.5 mm in order to reduce

stress concentration at the tip of the strut. The strut thickness had bounds of 0.025

mm to 0.25 mm. These bounds were placed on the strut due to considerations of

restenosis. Thicker stent struts typically have higher restenosis rates as compared to

thinner struts. The strut thickness also influences the section modulus of the strut. A

larger section modulus helps to reduce the stresses present. The strut wall thickness

was given the same bounds as the wall thickness in order to influence the section

modulus.

The strut design study had 41 iterations. The parametrically designed strut

reduced the maximum stresses to 7.5 MPa. Figure 21 shows the stress distribution in

the parametrically designed stent.
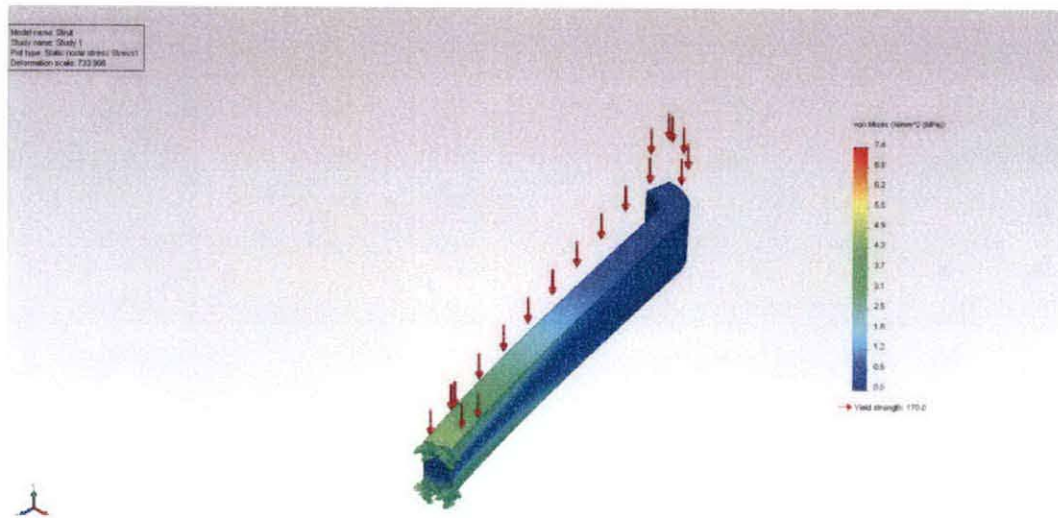
Figure 21. Stresses within the parametrically designed strut.

The connecting bridges were also parametrically designed. The bridge was designed in the same manner as the strut. An initial sketch of the bridge was created with bounds on the length and width. The constraints on the length and width allow the bridge to connect with the adjacent struts. The wall thickness was also constrained to be equal to the wall thickness of the strut. The constraint on the wall thickness allows for a uniform transition between the strut and the bridge.

The bridge leg length was given bounds of 0.0125 mm to 1.125 mm. These bounds provided a constraint that prevented the bridge from colliding with the adjoining strut. The bridge half width controlled half of the bridge thickness. This dimension was given bounds of 0.075 mm to 0.125 mm. An equation that sets the full bridge thickness to two times this dimension was created to control the full bridge thickness.

The bridge design study contained 9 combinations of variables. The bridge was loaded and meshed similar to the strut. The fine mesh option was used to create a high quality mesh. The uniformly distributed pressure of 0.016 MPa was applied to the bridge. Both ends of the bridge were fixed in order to mimic the connections to the stent struts. Figure 22 shows the bridge mesh and loading conditions. The green arrows indicate constrained boundary conditions and the red arrows indicate the uniformly distributed pressure.
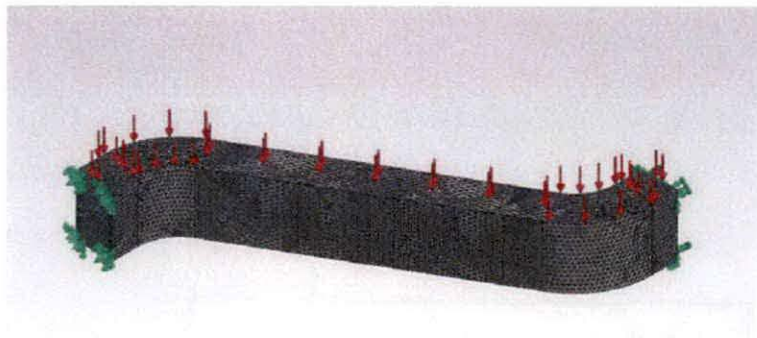
Figure 22. Bridge loading and boundary conditions.

The bridge had a maximum stress of 0.856 MPa as shown in Figure 23. The parametric design study showed that this bridge configuration is capable of minimizing the maximum bridge stresses.
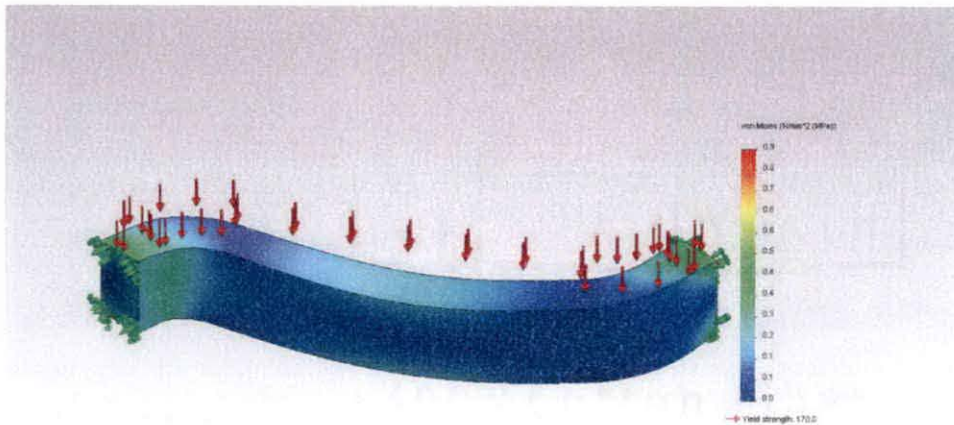
Figure 23. Bridge stresses (MPa).

The strut design and the bridge design were combined to create the final stent geometry. In order to create a stent in SolidWorks®, the stent must first be modeled using two dimensional modeling techniques to model the stent in its unwrapped configuration. A stent in its unwrapped configuration has a width equal to the wrapped diameter. The circumference of the stent can be defined using the conventional circle circumference equation.

$$C = \pi d \tag{44}$$

Where:

C is the stent circumference or the width of the unwrapped stent

d is the wrapped stent diameter

The struts were aligned in a pattern that gave the stent a circumference similar to those of stent A and stent B. It was only necessary to model two rows of struts due to symmetry.

The unwrapped configuration was then wrapped inside a hollow three dimensional tube. The inside diameter of the tube had a diameter equal to the unwrapped circumference divide by pi. This diameter is also equal to the wrapped stent diameter.

$$d = \frac{C}{\pi} \qquad (45)$$

Where:

d is the hollow tube inside diameter and the stent diameter

C is the stent circumference

The wrapped stent was given a wall thickness equal to the thickness found in the parametric design study (0.25 mm). The hollow tube was then cut from the stent to reveal the wrapped stent geometry. This final stent will be referred to as Stent C in this paper.
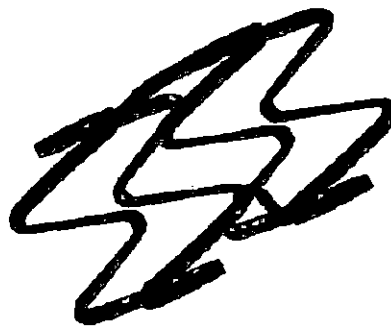
Figure 24. Final stent c in the wrapped configuration.

Stent Materials

Nitinol, 316L stainless steel, and poly-L-lactid acid (PLLA) were chosen for

stent materials. These three materials are representative of commonly used

biocompatible stent materials.

Nitinol is an exotic shape memory alloy. It consists of a mixture of 50%

nickel and 50% titanium. This material has an unusual unloading pattern due to the

shape memory effect. Figure 4 in Chapter II shows the typical stress and strain

unloading path for Nitinol. Nitinol is able to recover large strains due to a mixture of

austenitic and martensitic grain structures. The ratio of the austenite and martensite

grains change when undergoing stress. The built-in Nitinol subroutine was used to

model the shape memory effect. The subroutine required the material properties for

the austenite and martensite grain structures to be entered. The values are shown in

Table 4 (Santillo, 2008).

Table 4

Nitinol Material Values

Material Properties	Property Description	Value
E_A	Austenite Elastic Modulus	35,877 MPa
ν_A	Austenite Poisson's Ratio	0.33
E_M	Martensite Elastic Modulus	24,462 MPa
ν_M	Martensite Poisson's Ratio	0.33
ε^L	Transformation Strain	0.0555
$\left(\dfrac{\delta\sigma}{\delta T}\right)$	$\left(\dfrac{\delta\sigma}{\delta T}\right)$ Loading	6.7
σ_L^S	Start of Transformation Loading	489 MPa
σ_L^E	End of Transformation Loading	572 MPa
T_0	Temperature	22 °C
$\left(\dfrac{\delta\sigma}{\delta T}\right)_U$	$\left(\dfrac{\delta\sigma}{\delta T}\right)$ Unloading	6.7
σ_U^S	Start of Transformation Unloading	230 MPa
σ_U^E	End of Transformation Unloading	147 MPa
σ_{CL}^S	Start of Transformation Stress	0.0
ε_V^L	Volumetric Transformation Strain	0.0474

Austenitic 316L stainless steel was also chosen as a stent material. Medical grade 316L stainless steel has the alloying components presented in Table 5 (The A to Z of Materials, 1999).

Table 5

316L Stainless Steel Alloying Elements and Their Percentages

	C	Mn	Si	P	S	Cr	Mo	Ni	N
%	0.03	2.0	0.75	0.045	0.03	18.0	3.00	14.0	0.10

The Ramberg-Osgood material model was used to determine the elastic/plastic response of the 316L stainless steel (Charalambides, 2011). This model is also known as a deformation plasticity model.

$$\varepsilon = \frac{\sigma}{E} + \alpha \frac{\sigma_o}{E} \left(\frac{\sigma}{\sigma_o} \right)^n \tag{46}$$

Where:

ε is the strain

σ is the stress

σ_o is the yield stress

$\alpha \frac{\sigma_0}{E}$ is the yield offset

E is the elastic modulus

n is the strain hardening exponent

Yield strength of 375 MPa and ultimate tensile strength of 474 MPa was used for stent grade 316L stainless steel (Bargiggia, 2008). Table 6 shows a summary of the material properties for 316L stainless steel.

Table 6

316L Stainless Steel Material Properties

E	v	σ_0	σ_{UTS}	n	$\alpha\dfrac{\sigma_0}{E}$
200,000 MPa	0.33	375 MPA	474 MPa	5	0.002

PLLA is a biodegradable polymer that has begun to be used in cardiovascular stents. This material is known to completely biodegrade within 24 months of stent insertion. PLLA can be modeled using a second order hyperelastic strain energy function.

$$U = C_{10}(I_1 - 3) + C_{20}(I_1 - 3)^2 + C_{01}(I_2 - 3) + C_{02}(I_2 - 3)^2 + C_{11}(I_1 - 3)(I_2 - 3) \quad (47)$$

Where:

U is the incompressible strain energy function

C is a material property constant

I_1 and I_2 are Cauchy strain invariants

The hyperelastic constants are shown in Table 7 (Masia, 2008).

Table 7

PLLA Hyperelastic Constants (MPa)

C_{10}	C_{01}	C_{02}	C_{20}	C_{11}
-2799.14	2913.45	27,122.10	-515.45	-21,168.36

Stent Crimping and Expansion

Stent crimping and expansion are necessary in order to add residuals stresses to the stent materials. Crimping and expansion take advantage of material plasticity to increase radial strength. Residual stresses from crimping and expansion are present in the stent even in a no load condition. It is important to model to accurately model these residual stresses in order to properly define the *in-vivo* conditions. The Abaqus® adjustable rigid torus (ART) plugin was used to control both stent crimping and stent expansion. The ART plugin uses cylindrical displacement boundary conditions and contact controls to control both stent crimping and expansion. The displacement boundary conditions cause the rigid cylinder radius to either increase (balloon expansion) or decrease (crimping). Balloon expansion uses a position displacement vector to increase the rigid cylinder's radius; while a crimping contact uses a negative displacement vector to decrease the radius. The user specifies the starting and ending cylinder radius as well as the contact type. Figure 25 shows the graphical input for the ART plugin.

	Number of Analysis Steps:	2				
Step	R_start	r_start	R_end	r_end	Contact Type	
Step-1	1e+20	2.5	1e+20	1.75	Catheter	
Step-2	1e+20	1.0	1e+20	2.125	Balloon	

Visualize the user-defined rigid torus surface

Starting point of the sweeping path (x,y,z)   0.0,0.0,0.0

Length of Visualization surface   0

	Number of Elements
Around circumference of r	20
Around circumference of R	100

Note: When r_start is equal to zero, the rigid surface will intelligently detect the correct radius.
   If a number is given, the plug-in will use it as the starting radius.
   When r_end is equal to zero, radius r_start remains constant.

Note: When using parallel processing on a cluster with physically distinct memory directly specify r_start.
   Intelligent radius detection algorithm may not work correctly in this situations

Figure 25. Adjustable rigid torus contact definition window.

The user also specifies the stent contact surfaces. The contact surfaces define

the points on the stent in which the rigid cylinder contacts. Typically, the inner stent

surface is defined for balloon contact and the outer stent surface is defined for

crimping contact. Figure 29 gives an example of a balloon rigid cylinder and a

crimping rigid cylinder.

(a)   (b)
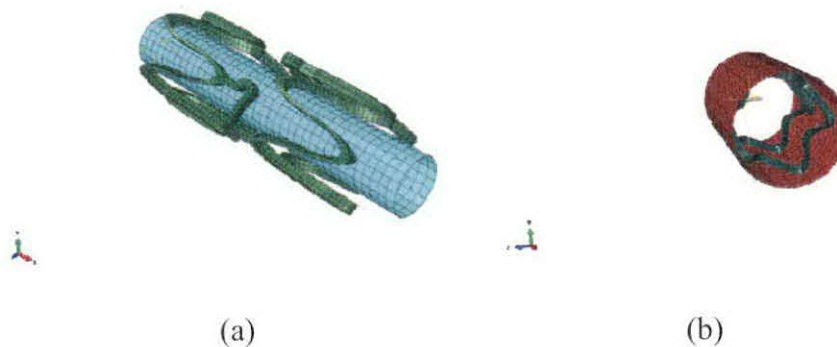
Figure 26. (a) balloon contact and (b) crimping contact.

Different crimping/expansion strategies were needed for 316L stainless steel and Nitinol, respectively. The stents were meshed using 8 node C3D8R hexahedral brick elements as prescribed in the literature (Rebelo, Fu, & Lawrenchuk, 2008). Global seeds of 0.175 and 0.1755 were used to facilitate the replicates in the statistical analysis. The 316L stainless steel required that the ART plugin perform both crimping and balloon expansion. A boundary condition that restrained linear translations in the axial (X axis) direction was added to one nodal point on the stent. This boundary condition eliminated a rigid body translation due to the crimping and expansion forces. The stents were crimped to a radius of 1.75 mm. The stents were first crimped to a radius of 1.75 mm. Figure 27 shows the three stents in their crimped configuration.

(a)   (b)   (c)

Figure 27. Crimped configurations for (a) stent a, (b) stent b, and (c) stent c.

A balloon contact was then used to expand the stents from the crimped profile to the expanded diameter. The same stent boundary conditions from the crimping step were used during expansion. The rigid torus representing the expansion balloon was displaced to a radius of 2.15 mm. The cylinder was then displaced with a

negative vector. The same balloon contact was used to control the stent surface. The negative balloon vector is analogous to balloon retraction after stent expansion. This was a crucial step in the stent expansion simulation because 316L stainless steel stents elastically recoil after expansion. The elastic recoil causes the stent to experience a small loss in expanded diameter and also a small decrease in residual stresses after expansion.

Nitinol was allowed to self-expand due to its shape memory properties. Nitinol stents have the unique ability to recover their original diameter after crimping. Devices called sheaths are used to prevent the Nitinol stent from recovering its shape until arterial insertion. The sheath is removed from the stent after insertion, allowing the Nitinol stent to self-expand within the artery. The ART plugin was used to simulate both the crimping tool and the sheath. A node on the stent was constrained in the axial direction in order to prevent unwanted rigid motions. The rigid cylinder was negatively displaced using a crimp contact with the stent. The stent was crimped to a radius of 1.75 mm. The motion of the crimping tool was reversed using positive displacement vectors (the contact remained a crimping contact with the stent). The positive displacement represented the removal of the sheath. This removal allowed the Nitinol to recover the strain from the crimping step. Thusly, the stent returned to its original diameter.

Fatigue Loading and Study

Arterial blood pressure is periodic in nature. More specifically, it can be modeled using a sinusoidal function. Rebelo et al. found that the blood pressure has a mean value of 100 mmHg (0.013 MPa) (Rebelo, Fu, & Lawrenchuk, 2008). The blood pressure has a systolic value of 120 mmHg (0.016 MPa) and a diastolic value of 110 mmHg (0.010 MPa). Rebelo et al. also indicated that the blood pressure curve has a periodic frequency of 1.2 Hz. A sinusoidal function was developed using the data presented by Rebelo et al. The circular frequency of the function was calculated.

$$\omega = 2\pi f \tag{48}$$

Where:

ω is the circular frequency

f is the frequency

Blood pressure has a circular frequency of 7.53982 radians/second at a frequency of 1.2 Hz. The sinusoidal function was developed to have an alternating amplitude of 0.003 MPa around the mean blood pressure of 0.013 MPa.

$$f(x) = 0.003\sin(x) + 0.013 \tag{49}$$

The sinusoidal function was expanded using a Fourier series. The Fourier series expansion is defined below (Simulia).

$$a = A_o + \sum_{n=1}^{N} a_n \cos(n\omega)(t - t_o) + b_n \sin(n\omega)(t - t_o) \tag{50}$$

Where:

a is the Fourier expansion

A_0, A_n, and B_n are Fourier coefficients

t and t_0 are time values

The Fourier series coefficients were calculated to define the initial and

maximum amplitude of the blood pressure curve.

$$a_n = \frac{1}{\pi} \int_0^{2\pi} f(x) \cos(nx) \, dx \tag{51}$$

$$b_n = \frac{1}{\pi} \int_0^{2\pi} f(x) \sin(nx) \, dx \tag{52}$$

An n value of one was used in order to create one value for a_n and b_n.

$$a_n = \frac{1}{\pi} \int_0^{2\pi} (0.003 \sin(x) + 0.013) * \cos(x) \, dx = 0 \tag{53}$$

$$b_n = \frac{1}{\pi} \int_0^{2\pi} (0.003 \sin(x) + 0.013) * \sin(x) \, dx = 0.003 \tag{54}$$

The Fourier series becomes sinusoidal due to the fact that a_n is zero. The

cosine terms of the series can be ignored.

$$a = A_o + \sum_{n=1}^{N} b_n \sin(n\omega)(t - t_o) \tag{55}$$

The Fourier analysis indicated that the blood pressure is purely sinusoidal and

fluctuates around the mean value with an amplitude of 0.003 MPa. Rebelo et al.

found that the pressure can be model using a mean value of 0 MPa with amplitude

fluctuations of 0.003 MPa (Rebelo, Fu, & Lawrenchuk, 2008). This remains a purely

sinusoidal loading curve.

$$f(x) = 0.003\sin(x) \tag{56}$$

The Fourier coefficients remain at 0 MPa and 0.003 MPa, respectively. The

pressure amplitude change from positive to negative indicates that the blood pressure

induces tensile and compressive loading. Perry et al. found that this change from

tension to compression causes the stent to cycle from its expanded major diameter to

a smaller minor diameter (Perry, Oktay, & Muskivitch, 2002).

Perry also found that stent fatigue is primarily determined by the stent

geometry, material strength, and blood pressure loading. Therefore, for the sake of

simplicity, the artery and stent contact can be ignored. This method is

computationally efficient due to the elimination of contact matrix iterations and a

reduction in the number of systems of equations.

Pressure was applied to the inside of the stent as a periodic load using the

above stated Fourier expansion. Translations in the X, Y, and Z axes were

constrained on a node on both the proximal and distal ends of the stent. The

constrained boundary conditions prevented the stents from rotating.

A modified Goodman failure criterion is generally used for stent finite life

assessment. The Modified Goodman criterion is summarized in equation 57.

$$\frac{\sigma_a}{\sigma_e} + \frac{\sigma_m}{\sigma_{uts}} = 1 \tag{57}$$

Where:

σ_a is the alternating stress

σ_e is the material endurance strength

σ_m is the mean stress

σ_{uts} is the material ultimate tensile strength

Stress life theory was used to determine the number of reversible cycles of the

316L stainless steel stents. Stress life theory expands on the Modified Goodman

theory by taking stress amplitude and the material's ultimate tensile strength into

account when determining the cycle to failure.

$$S_f = aN^b \tag{58}$$

Equation 58 was used to solve the number of reversible loads until stent

failure.

$$a = \frac{(fS_{ut})^2}{S_e} \tag{59}$$

$$b = -\frac{1}{3}\log\left(\frac{fS_{ut}}{S_e}\right) \tag{60}$$

$$\sigma_a = \left|\frac{\sigma_{max} - \sigma_{min}}{2}\right| \tag{61}$$

$$N = \left(\frac{\sigma_a}{a}\right)^{\frac{1}{b}} \tag{62}$$

$$S_e = 0.5S_{uts} \tag{63}$$

The UTS value for 316L stainless steel was calculated to be 474 MPa

(Bargiggia, 2008). The fatigue strength fraction (f) was determined to be 0.9 due to

the material's ultimate tensile strength. The material's endurance strength (S_e) is half

of the ultimate tensile strength or 242.5 MPa. The 'a' value was calculated to be 776.099 MPa. The 'b' value was calculated to -0.085091 for 316L stainless steel.

The maximum principle stress at the beginning of the fatigue loading and the minimum principle stress at the end of the fatigue loading step were analyzed to determine the stress amplitude. Table 8 contains the stress amplitude for the 316L stainless steel stents.

Table 8

Stress Amplitude for 316L Stainless Steel Stents (MPa)

Stent Design	Replicate 1	Replicate 2
A	562.0	514.5
B	123.5	122.8
C	164.8	124.4

(a)

(b)

(c)

(d)

Figure 28. Stent a stress; (a) maximum principle stresses (replicate 1), (b) minimum

principle stress (replicate 1), (c) maximum principle stresses (replicate 2), and (d)

minimum principle stress (replicate 2)

Figure 28 shows that the stresses in stent A with 316L stainless steel as the

material are evenly distributed throughout the entire stent. It is hypothesized that

crack initialization could occur at any point within the stent. This wide spread crack

initialization could possibly lead to widespread crack propagation and total stent

failure. Widespread crack propagation would most likely lead to a loss of stent hoop

strength and stent collapse. It also shows a significant change in stent diameter. This

could possibly be caused by the thin nature of the struts which lead to a smaller

section modulus and higher deflection.
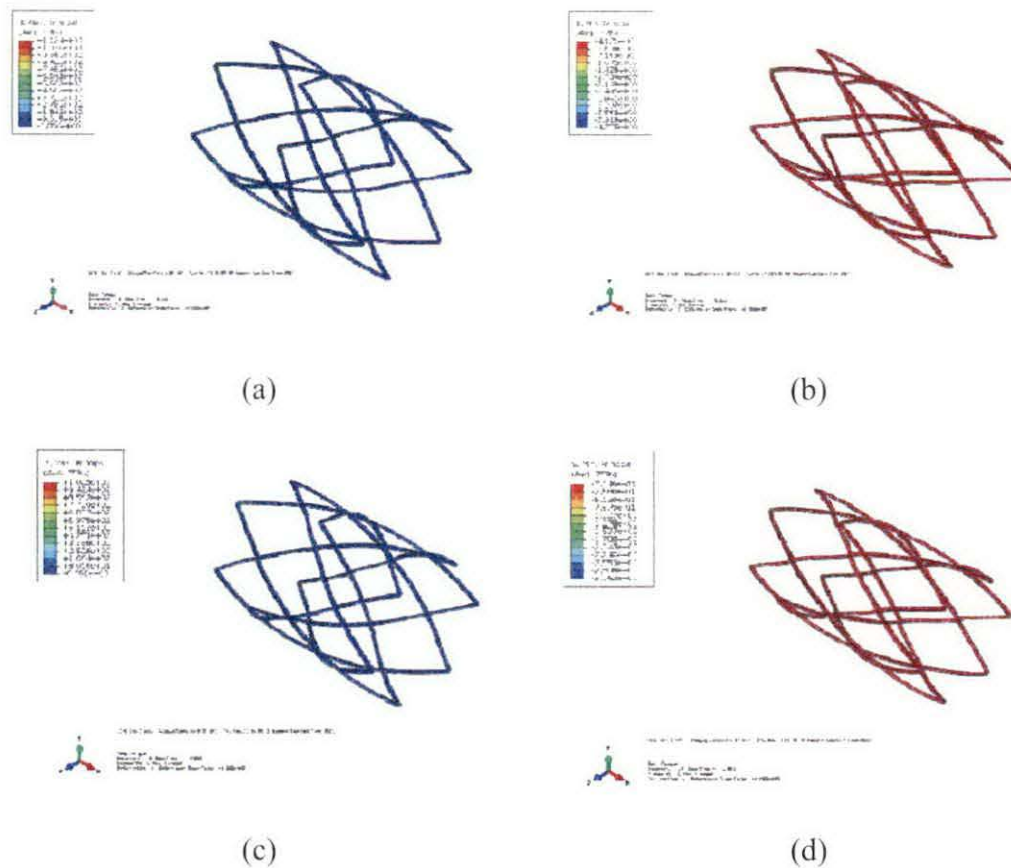

(a)

(b)

(c)

(d)

Figure 29. Stent b stress; (a) maximum principle stresses (replicate 1), (b) minimum

principle stresses (replicate 1), (c) maximum principle stresses (replicate 2), and (d)

minimum principle stresses (replicate 2)

Figure 29 shows stent B with 316L stainless steel at the material. Stresses are

concentrated along the inside of the struts. Stresses are also localized around the strut

and bridge connection. It can be safely assumed that crack initialization would occur

at the localized stress regions. The strut and bridge interface are stress concentration

points due to sharp corners produced from the transition from bridge to strut. This figure also shows relatively low stresses in the struts that are not adjacent to the bridges which lead to the viability of open stent designs. The struts would be able to maintain radial strength due to the low stresses in the struts.
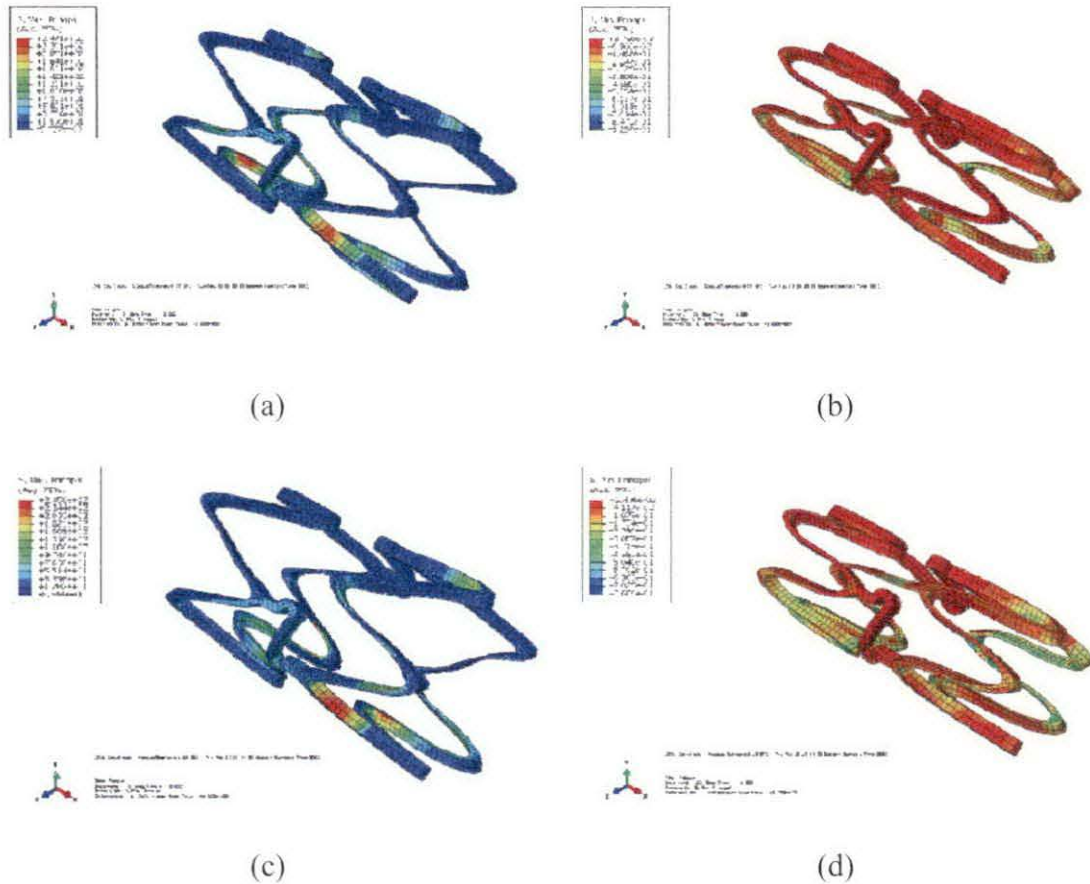

(a)

(b)

(c)

(d)
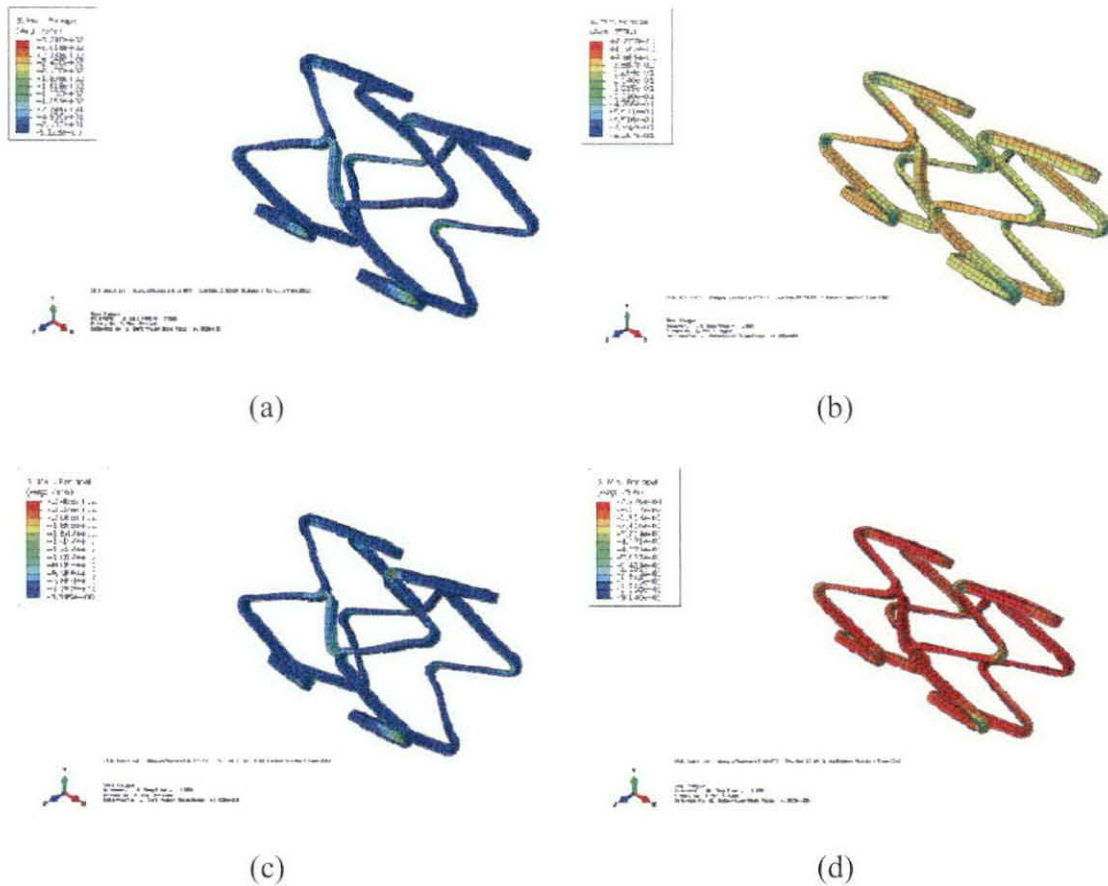
Figure 30.Stent C stress; (a) maximum principle stresses (replicate 1), (b) minimum principle Stresses (replicate 1), (c) maximum principle stresses (replicate 2), and (d) minimum principle stresses (replicate 2)

Figure 30 shows the stresses for stent c with 316L stainless steel as the material. Stresses are concentrated at the strut and bridge transition (similar to that of stent B). Crack initialization is hypothesized to begin at the transition.

Table 9 shows the fatigue life for the 316L stainless steel stents.

Table 9

Fatigue for 316L Stainless Steel Stents (number of cycles)

Stent Design	Replicate 1	Replicate 2
A	44.4	125.3
B	$2.4*10^9$	$2.6*10^9$
C	$8.0*10^7$	$2.2*10^9$

Nitinol exhibited low principle stresses during expansion and fatigue loading due to its stress/strain recovery. Therefore, strain life theory is suitable for accurately determining the finite life cycle of a Nitinol stent (Runciman, Xu, Pelton, & Ritchie, 2011).

$$\frac{\Delta \varepsilon}{2} = 61.7 N^{-\frac{1}{2}} \qquad (64)$$

Where:

$\Delta\varepsilon/2$ is the strain amplitude

N is the cycles until failure

Table 10 contains the strain amplitude for the Nitinol stents.

Table 10

Strain Amplitude for Nitinol Stents

Stent Design	Replicate 1	Replicate 2
A	$5.7*10^{-4}$	$5.7*10^{-5}$
B	$2.72*10^{-4}$	$2.25*10^{-4}$
C	$9.1*10^{-5}$	$9.1*10^{-5}$

The following figures show the strain locations for Nitinol based stents.

These figures begin on the next page.

(a)

(b)

(c)

(d)

Figure 31. Stent a strain; (a) maximum principle strain (replicate 1), (b) minimum principle strain (replicate 1), (c) maximum principle strain (replicate 2), and (d) minimum principle strain (replicate 2)

Figure 31 shows the strains for stent A with Nitinol as the material. Nitinol shows dissimilar results compared to 316L stainless steel for this stent. The strains are not uniformly distributed as the stresses were. The Nitinol based strains are located at the connection points between struts. This strain concentration is most likely due to the sharp transition between struts. Crack initialization would occur at these sharp transitions.

(a)

(b)

(c)

(d)

Figure 32. Stent b strain; (a) maximum principle strain (replicate 1), (b) minimum principle strain (replicate 1), (c) maximum principle strain (replicate 2), and (d) minimum principle strain (replicate 2)

Figure 32 shows that the strains for stent B (Nitinol as the material) are localized on the inside of the struts. These strains would act as crack propagation points. The high strain amplitude at these points would most likely lead to crack initialization and ultimately lead to stent failure.
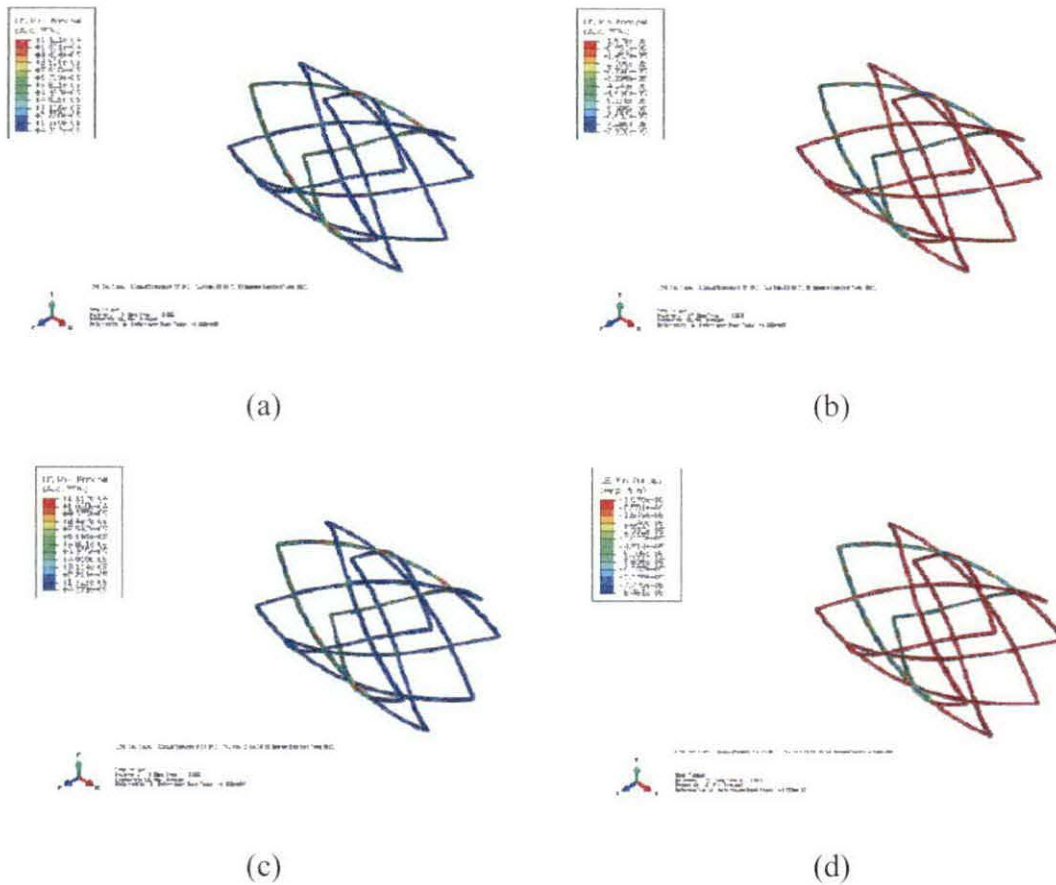
(a)

(b)

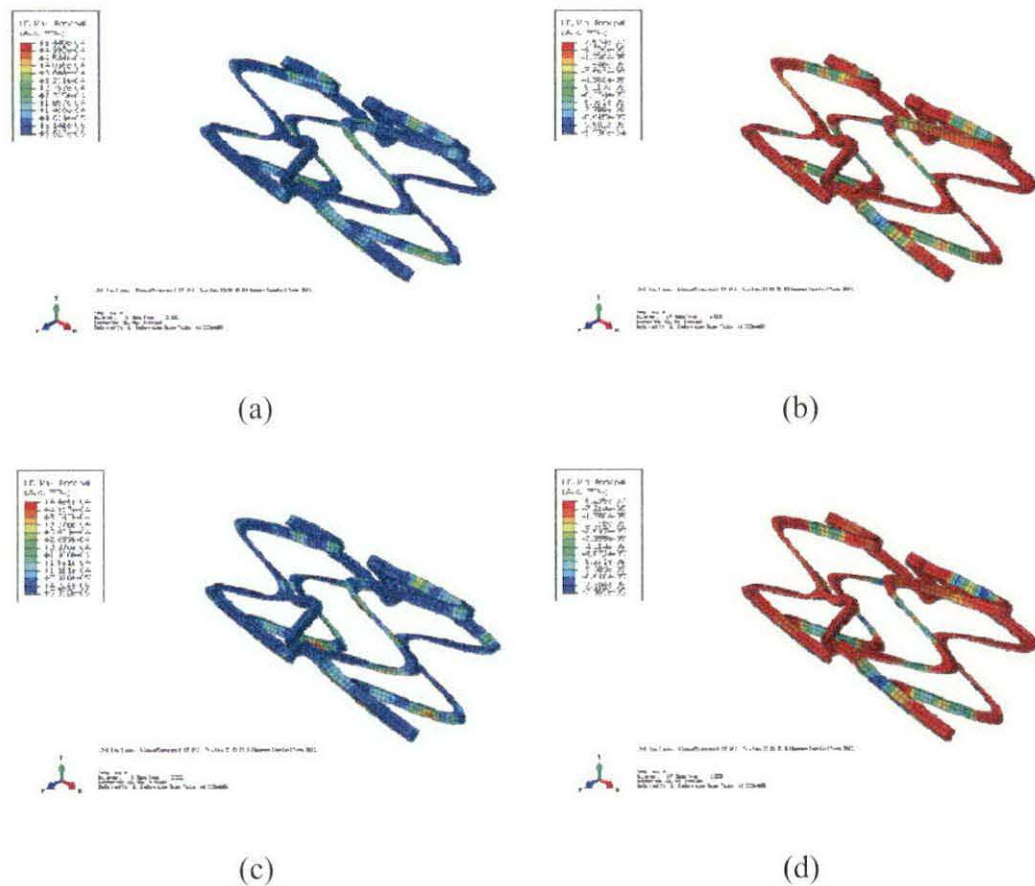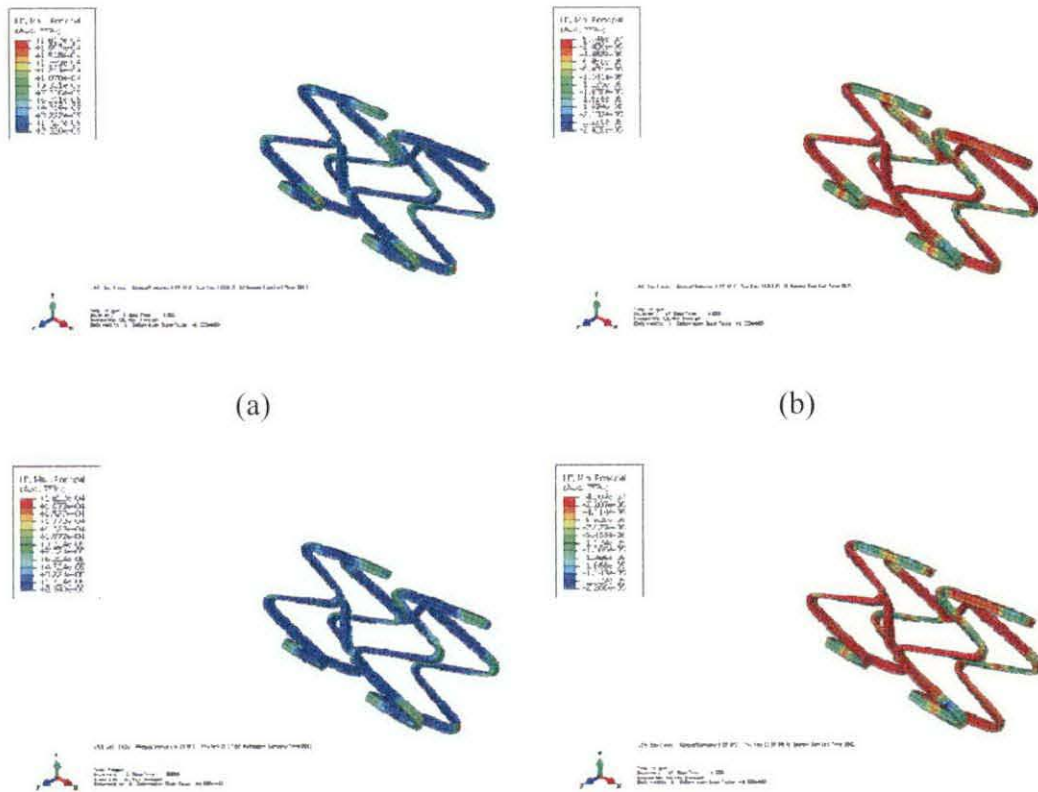
Figure 33. Stent C strain; (a) maximum principle strain (replicate 1), (b) minimum principle strain (replicate 1), (c) maximum principle strain (replicate 2), and (d) minimum principle strain (replicate 2)

Figure 33 shows that the strains for stent C are concentrated around the strut curvature. Cracks could form at these points.

Table 11 contains the cycles to failure for the Nitinol stents.

Table 11

Fatigue for Nitinol Stents (number of cycles)

Stent Design	Replicate 1	Replicate 2
A	$1.2*10^{12}$	$1.2*10^{12}$
B	$5.1*10^{10}$	$7.5*10^{10}$
C	$4.6*10^{11}$	$4.6*10^{11}$

PLLA was used as a control in this experiment because it has a known

biologically corrosive fatigue life. The human body completely absorbs a PLLA stent

within 24 months of insertion. The number of heart beat cycles until complete

absorption was calculated. Ten years is equal to 380,008,800 heart beat pulse cycles.

Dividing this value by ten yielded a yearly total of 38,000,880 cycles. Therefore, 24 months

is the equivalent of $7.6*10^7$ cycles.

Statistical Analysis

A 2^3 factorial design was created in order to understand the significance of

stent design and material selection on fatigue life. The factors for this study were

stent design and material. Different stent designs were stent A, stent B, and stent C.

The different materials were levels of 316L stainless steel, Nitinol, and PLLA.

Fatigue life was used as the response variable in the study. The study used two

replicates. Table 12 shows the combination table for the factorial design and

replicates.

Table 12

Factorial Design Combination Table with Response Variable

Stent Design	Material		
	SS316L	Nitinol	PLLA
Stent A	$4.4*10^1$	$1.8*10^{12}$	$7.6*10^7$
	$1.3*10^2$	$1.2*10^{12}$	$7.6*10^7$
Stent B	$2.4*10^9$	$5.1*10^{10}$	$7.6*10^7$
	$2.6*10^9$	$7.5*10^{10}$	$7.6*10^7$
Stent C	$8.0*10^7$	$4.6*10^{11}$	$7.6*10^7$
	$2.2*10^9$	$4.6*10^{11}$	$7.6*10^7$

An analysis of variance (ANOVA) was used to determine the main effects and

interactions. Table 13 shows the results from the ANOVA testing.

Table 13

ANOVA Output from Minitab

```
General Linear Model: Fatigue Life versus Stent Design, Material

Factor         Type   Levels  Values
Stent Design   fixed       3  A, B, C
Material       fixed       3  SS316L, Nitinol, PLLA


Analysis of Variance for Fatigue Life, using Adjusted SS for Tests

Source               DF       Seq SS       Adj SS       Adj MS      F      P
Stent Design          2    7.07423E+23  7.07423E+23  3.53711E+23  16.98  0.001
Material              2    1.77490E+24  1.77490E+24  8.87448E+23  42.60  0.000
Stent Design*Material 4    1.42178E+24  1.42178E+24  3.55446E+23  17.06  0.000
Error                 9    1.87502E+23  1.87502E+23  2.08335E+22
Total                17    4.09161E+24


S = 144338191246   R-Sq = 95.42%   R-Sq(adj) = 91.34%
```

A confidence value of 95% was used to interpret the results. The significance

interval (α) was 0.05 due to the 95% confidence. The p values were compared to the

significance interval. The factor stent design had a p value of 0.001. This is less than

the α value of 0.05. Therefore, the null hypothesis can be rejected and it can be safely

concluded that stent design is an important factor when determining fatigue life. The

significance of stent material was also determined. The factor stent material had a p

value of 0.000. This is also less than the α value, indicating a rejection of the null hypothesis. Stent material is a significant determinant in fatigue life. The interaction between stent design and material was also analyzed using the p value. The interaction (stent design*material in Table 13) had a p value of 0.000. The null hypothesis was rejected and the interaction is significant.

An analysis of residuals and normality showed that the data is not normally distributed. ANOVA is based upon the assumption that the residuals are normally distributed. Therefore, the aforementioned null hypothesis rejections may not be reliable.
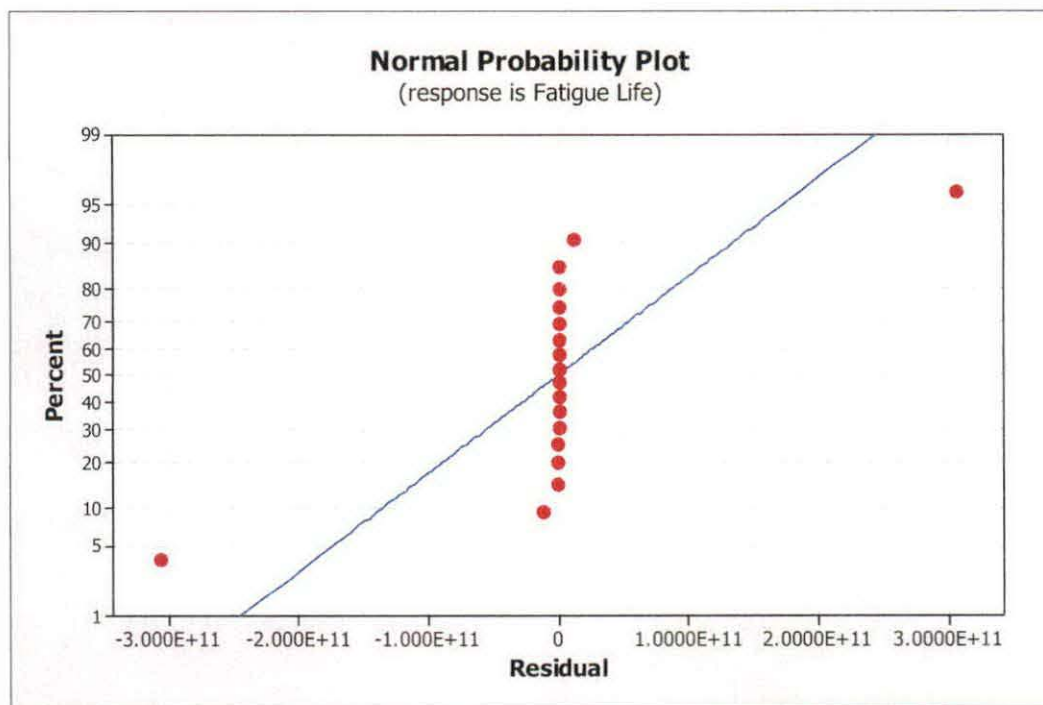
Figure 34. Normal probability plot versus residuals.
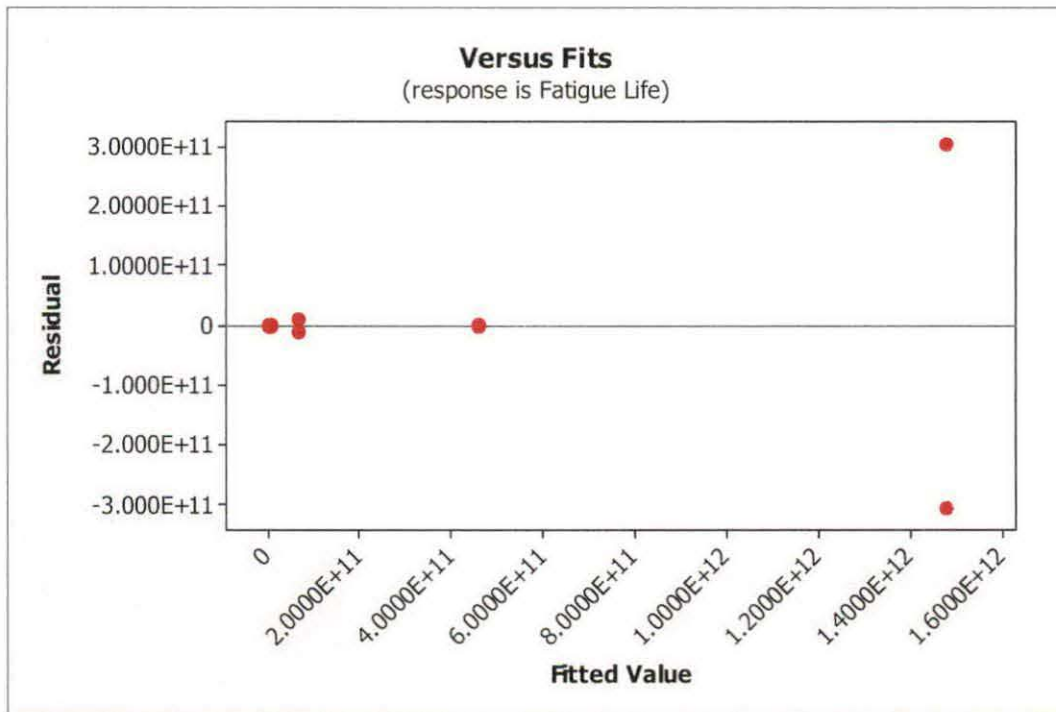
Figure 35. Fits versus residuals.

The non-normality in the data was caused by the constant corrosive fatigue life of PLLA. Mechanically speaking, PLLA is a poor material choice when maximizing fatigue life. PLLA does offer biological advantages due to its lowered restenosis rates. Removing PLLA from the analysis returned the residuals to a normal distribution. The P values were then recalculated without PLLA. Table 14 shows the recalculated ANOVA table.

Table 14

Recalculated ANOVA Table

General Linear Model: Fatigue Life versus Stent Design, Material

```
Factor        Type   Levels  Values
Stent Design  fixed      3   A, B, C
Material      fixed      2   Nitinol, SS316L
```

Analysis of Variance for Fatigue Life, using Adjusted SS for Tests

Source	DF	Seq SS	Adj SS	Adj MS	F	P
Stent Design	2	1.06113E+24	1.06113E+24	5.30567E+23	16.98	0.003
Material	1	1.32891E+24	1.32891E+24	1.32891E+24	42.52	0.001
Stent Design*Material	2	1.06807E+24	1.06807E+24	5.34037E+23	17.09	0.003
Error	6	1.87502E+23	1.87502E+23	3.12503E+22		
Total	11	3.64562E+24				

S = 176777459474   R-Sq = 94.86%   R-Sq(adj) = 90.57%

The p values were then re-analyzed to determine the significance of the factors. The re-analysis showed that the p values for the main effects as well as the interaction were less than the α value. The null hypothesis can be rejected indicating that the main effects and interactions are significant.

The recalculated probability plots showed normally distributed residuals. The normal distribution indicated model adequacy and that the null hypothesis can be reliably rejected.
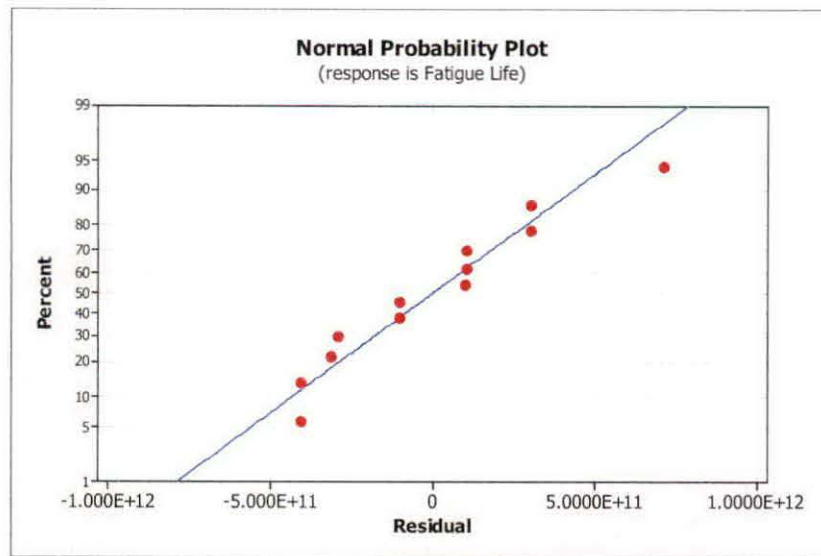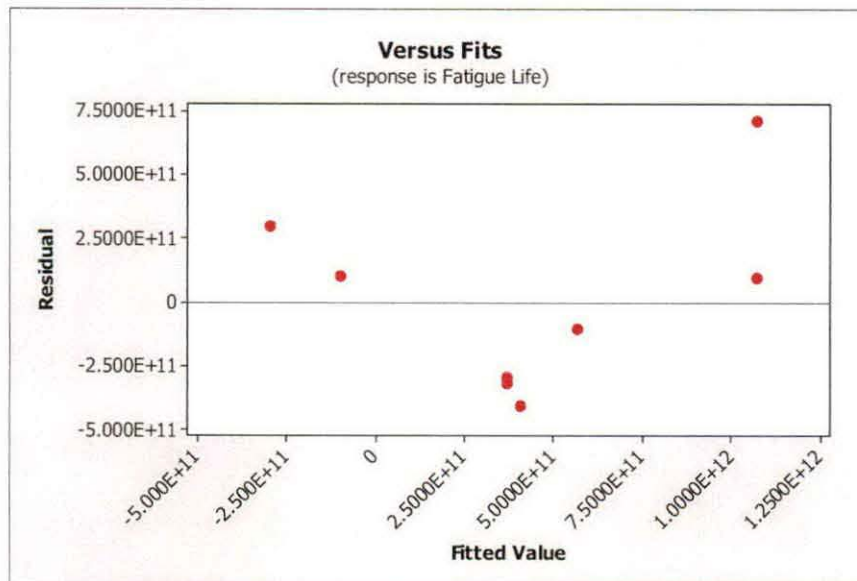
Figure 36. Recalculated normal probability plot.

Figure 37. Recalculated fits versus residuals plot.

One goal of any stent design to maximize the fatigue life so that the stent does not prematurely fail once the stent is placed *in-vivo*. The interaction plot presented in Figure 38 indicated that Nitinol maximizes the fatigue for all stent designs studied.

However, a single stent design did not independently maximize fatigue life. Stent A performed well using Nitinol as a material but performed poorly with 316L stainless steel as the material. This variance of performance from stent A indicates that the design is not a robust design. A robust stent should provide adequate fatigue performance utilizing a variety of materials. stent B and stent C provided more consistent performance utilizing both 316L stainless steel and Nitinol. The interaction plot shows that stent B had a higher fatigue life than stent C with 316L stainless steel as the material, while stent C had a higher fatigue life with 316L stainless steel.
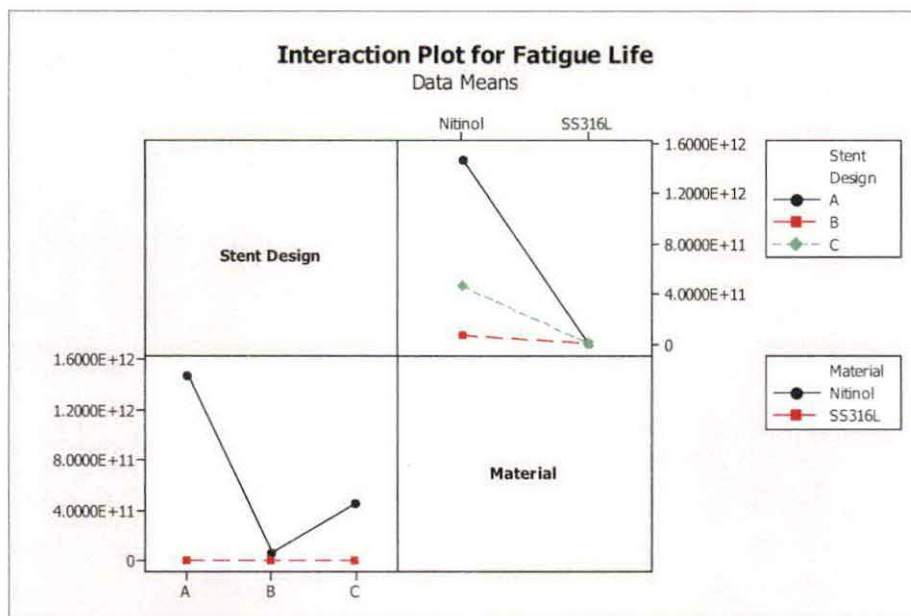

Figure 38. Interaction plot for fatigue life.

A Fisher least significant difference (LSD) analysis was also performed. The Fisher LSD method compares the mean of the treatments using one way ANOVA techniques. This

method is useful in finding the similarities and dissimilarities between treatments of a factor.

Figure 39 shows the Fisher LSD output for stent design.

```
Stent
Design  N         Mean  Grouping
A       4  7.38825E+11  A
C       4  2.30170E+11  A
B       4  32969075000  A
```

Figure 39. Fisher LSD grouping for stent designs.

The results of the Fisher LSD for stent design showed that all stent designs are

similar because they belong to the same grouping. Figure 40 shows the Fisher LSD

groupings for the treatments of the material factor.

```
Material  N         Mean  Grouping
Nitinol   6  6.66768E+11  A
SS316L    6  1208403262   B
```

Figure 40. Fisher LSD grouping for materials.

Figure 40 shows that the materials were placed in two distinct groupings. The

difference in grouping indicates that the different material treatments are dissimilar.

This dissimilarity means that one material provides better fatigue performance over

the other. Nitinol provides maximum fatigue life compared to 316L stainless steel.

Chapter Five

Summary

In this research, the effects of stent design and material on fatigue life were analyzed. Combinations of three stent designs (see Chapter IV) and three materials (316L stainless steel, Nitinol, and PLLA) were tested using Abaqus® finite element analysis software. A stent geometry was also created using the parametric design capabilities of SolidWorks®. The stents models were crimped and then expanded to add appropriate residual stresses. A sinusoidal fatigue load that was equivalent to blood pressures was then applied to the stents. The maximum/minimum principle stresses and maximum/minimum principle strains were analyzed in order to calculate the fatigue load amplitude. The number of fully reversible loads to failure was calculated using stress life theory and strain life theory. An analysis of variance was used to determine the significance of stent design and material on fatigue life.

Conclusion

The ANOVA analysis showed that the stent design, material, and the interaction between the two are significant determinants of fatigue life. A Fisher LSD showed that the stent designs produced similar results. The deciding factor in stent fatigue life is stent material. Stent design only produce moderate changes in fatigue life while material produced a significant change in fatigue life. Designs need to be robust so that a variety of materials can be used. For example, if future research

found that Nitinol was not biologically compatible, a robust stent design would be able to use 316L stainless steel with similar fatigue life.

The study found that Nitinol was the best material for maximizing fatigue life. However, fatigue life is not the only factor in the design of stents. PLLA was found to have an undesirable fatigue life due to its corrosive fatigue. However, PLLA is an emerging stent technology because of its favorable biological properties. PLLA may lead to lower restenosis and in-stent thrombosis. Metallic stents can lead to blood clots due to the polar attraction between the metal and blood cells (hence drug-eluting stents were introduced to provide anti-thrombotic agents). PLLA reduces the risk of blood clots by eliminating the polar attraction. It is thought that the artery will be completely healed within a few years of stent insertion. Therefore, stents may not need to be permanent arterial scaffolding. Therefore, PLLA may provide this advantage over its Nitinol and 316L counterparts.

The study found that material is the most significant factor in determining fatigue life. However, design is still a very important aspect of a stent's success. Stents also need a high amount of hoop strength (hoop strength is the stent's resistance to the circumferential stresses applied to the stent due to arterial loading). Struts with thicker struts have higher hoop strength (but can also have higher restenosis rates). Flexibility is also an important aspect of a stent's success. A stent must be flexible in order for it to travel on a guide wire through the cardiovascular tree to the offending artery. Open cell stents similar to Stents B and C were developed to add flexibility and maintain hoop strength.

Future Research

This research can be expanded to include further *in-vivo* simulations. The artery uhyper subroutine written in this thesis can be expanded to an Abaqus® vumat subroutine. The vumat subroutine is an Abaqus® explicit code that can be used to model nonlinear materials. Incorporating the vumat code will allow the stents to be expanded into an artery model. This thesis used Abaqus® implicit; therefore it was not possible to accurately solve the contact between the stent and artery. Abaqus® explicit will be better suited for solving the contact between the two dissimilar materials. The fatigue analysis can then be performed using *in-vivo* loading conditions.

An analysis of restenosis would also be an appropriate future work. The stent exerts a number of forces on the artery during deployment as well as during blood pressure cycling. The forces in turn induce stresses within the arterial wall layers. High stresses in the intimal layer can lead to wall shearing. Smooth muscle cells accumulate around the tear in attempt to heal the artery. The accumulation of smooth muscle cells can lead to lumen loss which causes restenosis. FEA can be used to determine the onset of restenosis in differing stent designs. The stresses within the artery model can be analyzed after the stent model is deployed. The average stresses in the artery can be used a determinant of stent compliance. Lower artery stresses would be an indicator of low restenosis rates while higher artery stresses would be indicative of high restenosis rates.

Bibliography

Bargiggia, U. (2008). *Stent Fatigue Life Prediction: An Analytical and Experimental Approach.* Department of Biomedical Engineering. University of Pavia.

Bennett, M. R. (2007). The Atherosclerotic Plaque Was Not Built in a Day: The Dynamic Nature of Plaque Progression and Instability. *Heart and Metabolism, 36,* 5-7.

Bobryshev, Y. V., Lord, R., & Warren, B. A. (1995). Calcified Deposit Formation in Intimal Thickenings of the Human Aorta. *Atherosclerosis, 118,* 9-21.

Bonsignore, C. (2010). Open Stent Design: Computer Methods for Cardiovasculare Devices 2010. *FDA/NHLBI/NSF Workshop on Computer Methods for Cardiovascular Devices.* Washington DC: FDA.

Briguori, C., Sarais, C., Pagnotta, P., Liistro, F., Montorfano, M., Chieffo, A., . . . Colombo, A. (2002). In-Stent Restenosis in Small Coronary Arteries. *Journal of the American College of Cardiology, 40*(3), 403-409.

Budynas, & Nisbett. (2006). *Shigley's Mechanical Engineering Design* (8th ed.). McGraw-Hill.

Centers for Disease Control and Prevention. (2010, December 21). *Heart Disease Facts.* Retrieved December 5, 2011, from Heart Disease: http://www.cdc.gov/heartdisease/facts.htm

Cervera, J. (2006). *Stent Design and Arterial Mechanics: Parameterization Tools Using the Finite Element Method.* Texas A&M University, Biomedical Engineering. College Station: Texas A&M University.

Charalambides, A. (2011). *Modeling of the Balloon-Stent-Vessel Expansion Mechanics.* Department of Mechanical Engineering. Baltimore: University of Maryland.

Chua, S. N., Mac Donald, B. J., & Hashmi, M. S. (2002). Finite-Element Simulation of Stent Expansion. *Journal of Materials Processing Technology, 120*(1), 335-340.

De Beule, M., Van Impe, R., Verhegghe, B., Seger, P., & Verdonck, P. (2006). Finite Element Analysis and Stent Design: Reduction of Dogboning. *Technology and Health Care, 14*, 233-241.

Di Mauro, P., Cisilino, A. P., & Pelossi, P. L. (2008). Finite Element Modeling of Alloys with Shape Memory for Use in Denistry. *Computational Mechanics*, 3317-3337.

Early, M., & Kelly, D. J. (2010). The Role of Vessel Geometry and Material Properties on the Mechanics of Stenting in the Coronary and Peripheral Arteries. *224*(3).

Ellis, S. G., & Holmes, D. R. (Eds.). (2000). *Strategic Approaches in Coronary Intervention* (2 ed.). Philadelphia: Lippincott Williams & Wilkins.

Fitzpatrick, L. A., Edwards, W. D., & Ingram, R. T. (1994). Diffuse Calcification in Human Coronary Arteries. *The Journal of Clinical Investiation, 94*, 1597-1604.

Forensic Medicine for Medical Students. (2010). *Sudden Cardiac Death and Coronary Artery Disease*. Retrieved December 19, 2011, from Pathology: http://www.forensicmed.co.uk/pathology/sudden-cardiac-death/sudden-cardiac-death-and-coronary-artery-disease/

Fox, C., Davies, M. J., & Webb-Peploe, M. M. (1973). Length of Left Main Coronary Artery. *35*.

Fung, Y. C. (Ed.). (2002). *Introduction to Bioengineering* (Vol. 2). River Edge, New Jersey: World Scientific.

Glagov, S. (1994). Intimal Hyperplasia, Vacular Modeling, and the Restenosis Problem. *Circulation, 89*, 2888-2891.

Gopal, S., Kim, S., Swift, R., & Choules, B. (2008). Fatigue Life Estimation of Nitinol Medical Devices. *Abaqus Users' Conference*. New Port, RI: Simulia.

Green, S. I., Schajer, G. S., Parker, D. R., & Post, A. J. (1995, November). In Vivo Measurement of Arterial Pre-Tension. *Medical and Biological Engineering and COmputing*.

Guyton, J. R., & Klemp, K. F. (1989). The Lipid-Rich Core Region of Human Atherosclerosis Fibrous Plaques: Prevalence of Small Lipid Droplets and Vesicles by Electron Microscopy. *The American Journal of Pathology, 134*(3), 705-717.

Hastings, G. W. (1992). *Cardiovascular Biomaterials.* London: Springer-Verlag.

Holzapfel, G. A., Sommer, G., Gasser, C. T., & Regitnig, P. (2005). Determination of Layer-Specific Mechanical Properties of Human Coronary Arteries with Nonatherosclerotic Intimal Thickening and Related Constitutive Modeling. *289.*

Holzapfel, G. A., Sommer, G., Gasser, C. T., & Regitnig, P. (2005). Determination of Layer-Specific Mechanical Properties of Human Coronary Arteries with Nonatherosclerotic Intimal Thickening and Related Constitutive Modeling. *American Journal of Physiology: Heart and Circulatory Physiology, 289,* 2048-2058.

Hsiao, H. M., Nikanorov, A., Prabhu, S., & Razavi, M. K. (2009). Respiration-Induced Kidney Motion on Cobalt-Chromium Stent Fatigue Resistance. *Journal of Biomedical Materials Research.*

Huang, H., Virmani, R., Younis, H., Burke, A. P., Kamm, R. D., & Lee, R. T. (2001). The Impact of Calcification on the Biomechanical Stability of Atherosclerotic Plaques. *Circulation, 103,* 1051-1056.

Hutton, D. V. (2004). *Fundamentals of Finite Element Analysis.* McGraw-Hill.

Kandzari, D. E., Tcheng, J. E., & Zidar, J. P. (2002). Coronary Artery Stents: Evaluating New Designs for Contemporary Percutaneous Intervention. *Catheterization and Cardiovascular Interventions, 56,* 562-576.

Kornowski, R., Hong, M. K., Tio, F. O., Bramwell, O., Wu, H., & Leon, M. B. (1998). In-Stent Restenosis: Contributions of Inflammatory Responses and Arterial Injury to Neointimal Hyperplasia. *Journal of the American College of Cardiology, 31*(1), 224-230.

Lai, W. M., Rubin, D., & Krempl, E. (2010). *Introduction to Continuum Mechanics* (4 ed.). Oxford: Elsevier.

Li, J., Lu, Q., Xie, Z., & Li, Y. (2010). Fatigue Life Analysis and Experimental Verification of Coronary Stent. *Heart and Vessels, 25*(4), 333-337.

Li, N., & Gu, Y. (2005). Parametric Design Analysis and Shpe Optimization of Coronary Artery Stent Structure. *World Congresses of Structural and Multidisciplinary Optimization.* Rio de Janeiro,Brazil.

Lim, I. A. (2004). Biocompatibility of Stent Materials. *11*.

Maher, E., Creane, A., Sultan, S., Hynes, N., & Lally, C. (2009). Tensile and Compressive Properties of Fresh Human Carotid Atherosclerotic Plaques. *Journal of Biomechanics, 7*(32).

Marrey, R. V., Burgermeister, R., Grishaber, R. B., & Ritchie, R. O. (2006). Fatigue and Life Prediction for Cobalt-Chromium Stents: A Fracture Mechanics Analysis. *Biomaterial, 27*, 1988-200.

Mase, G. E. (1970). *Schaum's Outlines: Continuum Mechanics.* New York: McGraw-Hill.

Masia, C. (2008). *Constitiutive Modelling of a Biodegradable Polymer (Poly-L-Lactic Acid) for Endovascular Applications.* University of Pavia, Biomedical Engineering. Pavia, Italy: University of Pavia.

Migliavacca, F., Petrini, L., Auricchio, F., & Dubini, G. (2003). Deployment of an Intravascular Stent in Coronary Stenotic Arteries: A Computational Study. *Summer Biobioengeering Conference.* Key Biscayne, Fl.

Migliavacca, F., Petrini, L., Massarotti, P., Schievano, S., Auricchio, F., & Dubini, G. (2004). Stainless and Shape Memory Alloy Coronary Stents: A Computational Study on the Interaction with the Vessel Wall. *Biomechanics and Modeling in Mechanobiology, 2*.

Mortier, P. (2010). Computer Modelling of Coronary Bifuraction Stenting.

Perry, M., Oktay, S., & Muskivitch, J. C. (2002). Finite Element Anlaysis and Fatigue of Stents. *Minimally Invasive Therapy and Allied Technologies, 11*(4), 165-171.

Petrini, L., Migliavacca, F., Dubini, G., & Auricchio, F. (2003). Numerical Analysis of Vascular Stents Exploiting Shape-Memory-Alloy Behavior. AIMETA Congress of Theoretical and Applied Mechanics.

Poerner, T. C., Haase, K. K., Wiesinger, B., Wiskirchen, J., & Duda, S. H. (2002). Drug-Coated Stents. *Minimally Invasive Therapy and Allied Technologies, 11*(4), 185-192.

Raines, E. W., & Ross, R. (1995). Biology of Atherosclerotic Plaque Formation: Possible Role of Growth Factors in Lesion Development and the Potential Impact of Soy. *The Journal of Nutrition*, 624S-630S.

Rebelo, N., Fu, R., & Lawrenchuk, M. (2008). Study of a Nitinol Stent Deployed into Anatomically Accurate Artery Geometry and Subjected to Realistic Service Loading. *Journal of Materials Engineering and Performance, 18*(5-6), 655-663.

Rensing, B. (2007). *Handbook of Coronary Stents* (4th ed.). (P. W. Serruys, Ed.) Martin Dunitz.

Ross, R. (1993, April 29). The Pathogenesis of Atherosclerosis: A Perspective for the 1990s. *Nature, 362*, 801-809.

Ross, R. (1999). Atherosclerosis: An Inflammatory Disease. *Mechanisms of Disease, 340*(2).

Runciman, A., Xu, D., Pelton, A. R., & Ritchie, R. O. (2011). An Equivalent Strain/Coffin-,amsopm Approach to Multiaxial Fatigue and Life Prediction in Superelastic Nitinol Medical Devices. *Biomaterials*.

Santillo, M. (2008). *Fracture and Crack Propagation Study of a Superficial Femoral Artery Nitinol Stent.* University of Pavia.

Simulia. (n.d.). Abaqus Analysis User's Manual.

Simulia. (n.d.). Abaqus Theory Manual.

Simulia Centrail. (2011). *Adjustable Rigid Torus (ART).* (Simulia) Retrieved January 2, 2012, from Extensions for Abaqus: http://www.simulia.com/products/rsurf.html

Sirol, M. (2006). Atherosclerosis Plaque Imaging and Characterization Using Magnetic Resonance Imaging. *US Cardiology*, 1-5.

Suri, J. S., Yuan, C., Wilson, D. L., & Laxminarayan, S. (2005). *Plaque Imaging: Pixel to Molecular Level.* Amsterdam: IOS Press.

Suter, Y., Schoenenberger, W., Toggweiler, S., Jamshidi, P., Resink, T., & Erne, P. (2009). Intravascular Ultrasound-Based Left Main Coronary Artery Assessment: Comparision Between Pullback from Left Anterior Descending and Circumflex Arteries. *21*(9).

Tang, D., Yang, C., Zheng, J., Woodard, P. K., Saffitz, J. E., Sicard, G. A., . . . Yuan, C. (2005). Quantiying the Effect of Plaque Structure and Material Properties on Stress Distributions in Human Atherosclerotic Plaques Using FSI Models. *127*.

The A to Z of Materials. (1999). *Stainless Steel-Grade 316L-Properties, Fabrication, and Applications.* Retrieved February 21, 2012, from The A to Z of Materials: http://www.azom.com/article.aspx?ArticleID=2382#_Composition

Timmins, L. H., Moreno, M. R., Meyer, C. A., Criscione, J. C., Rachev, A., & Moore, J. E. (2007). Stented Artery Biomechanics and Device Design Optimization. *Medical and Biological Engineering and Computing, 45*, 505-513.

Tong, R., & Rossettos, J. N. (2008). *Finite Element Analysis: Basic Techniques and Implementation.* Mineola, NY: Dover Publications.

U.S. Department of Health and Human Services. (2010). Non-Clinical Engineering Tests and Recommended Labeling for Intravascular Stents and Associated Delivery Systems. *Guidance for Industry and FDA Staff.*

Wang, H. H. (2001). Analytical Models of Atherosclerosis. *Journal of Atherosclerosis Research, 1*(7).

Wriggers, P., & Nackenhorst, U. (2006). *Analysis and Simulation of Contact Problems* (Vol. 27). Berlin: Springer.

Zahedmanesh, H., & Lally, C. (2009). Determination of the Influence of Stent Strut Thickness Using the Finite Element Method: Implications for Vascular Injury and In-Stent Restenosis. *Medical and Biological Engineering and Computing, 47*, 385-393.

Appendix A

Stent Design Fisher LSD

One-way ANOVA: Fatigue Life versus Stent Design

Source	DF	SS	MS	F	P
Stent Design	2	1.06113E+24	5.30567E+23	1.85	0.213
Error	9	2.58448E+24	2.87165E+23		
Total	11	3.64562E+24			

S = 535877572920   R-Sq = 29.11%   R-Sq(adj) = 13.35%

Level	N	Mean	StDev
A	4	7.38825E+11	8.88943E+11
B	4	32969075000	36541239580
C	4	2.30170E+11	2.64460E+11

Individual 95% CIs For Mean Based on Pooled StDev

Level   -+---------+---------+---------+--------

```
A                    (------------*-----------)

B        (------------*------------)

C         (------------*-----------)

         -+---------+---------+---------+--------
     -5.0E+11      0  5.00E+11  1.00E+12
```

Pooled StDev = 535877572920

Grouping Information Using Fisher Method

Stent

Design N   Mean Grouping

A   4 7.38825E+11 A

C   4 2.30170E+11 A

B   4 32969075000 A

Means that do not share a letter are significantly different.

Fisher 95% Individual Confidence Intervals

All Pairwise Comparisons among Levels of Stent Design

Simultaneous confidence level = 88.66%

Stent Design = A subtracted from:

Stent

Design	Lower	Center	Upper
B	-1.56304E+12	-7.05856E+11	1.51327E+11
C	-1.36584E+12	-5.08655E+11	3.48528E+11

Stent

Design   --+---------+---------+---------+-------

B   (-----------*-----------)

C   (-----------*-----------)

         --+---------+---------+---------+-------

      -1.4E+12 -7.0E+11   0 7.00E+11

Stent Design = B subtracted from:

Stent

Design   Lower   Center   Upper

C   -6.59982E+11 1.97201E+11 1.05438E+12

Stent

Design   --+---------+---------+---------+-------

C   (-----------*-----------)

          --+---------+---------+---------+-------

     -1.4E+12 -7.0E+11   0 7.00E+11

.

Material Fisher LSD

One-way ANOVA: Fatigue Life versus Material

Source	DF	SS	MS	F	P
Material	1	1.32891E+24	1.32891E+24	5.74	0.038
Error	10	2.31671E+24	2.31671E+23		
Total	11	3.64562E+24			

S = 481322062464 R-Sq = 36.45% R-Sq(adj) = 30.10%

Level   N   Mean   StDev

Nitinol 6 6.66768E+11 6.80691E+11

SS316L 6   1208403262   1299836359

        Individual 95% CIs For Mean Based on Pooled StDev

Level   -+---------+---------+---------+--------

Nitinol   (----------*----------)

SS316L   (----------*----------)

        -+---------+---------+---------+--------

       -4.0E+11   0 4.00E+11 8.00E+11

Pooled StDev = 481322062464

Grouping Information Using Fisher Method

Material N   Mean Grouping

Nitinol 6 6.66768E+11 A

SS316L   6   1208403262   B

Means that do not share a letter are significantly different.

Fisher 95% Individual Confidence Intervals

All Pairwise Comparisons among Levels of Material

Simultaneous confidence level = 95.00%

Material = Nitinol subtracted from:

Material	Lower	Center	Upper
SS316L	-1.28474E+12	-6.65559E+11	-4.63787E+10

```
Material  ------+---------+---------+---------+---

SS316L    (------------*-----------)

          ------+---------+---------+---------+---
         -1.0E+12  -5.0E+11      0  5.00E+11
```

Appendix B

Appendix C provides a tutorial for using Abaqus[®]. This tutorial shows the modeling and analysis of the three dimensional artery model using the uhyper subroutine written in this thesis (see Appendix A for source code).

When first opening Abaqus[®], you will see the Start Session window.

Figure C1. Start Session Window.

Choose With Standard/Explicit Model to start a new analysis. It is important to set a work directory. The work directory is a folder where all files related to the analysis are stored. Chose File → Set Work Directory. Browse to a folder where you would like Abaqus[®] to save the files.

Double click on parts (left side browser bar). A Create Part window will appear. Choose a 3D solid extrusion. The approximate shape is 20. Note that there

are no units. It is important to keep track of the units. The units for this tutorial are mm and MPa.
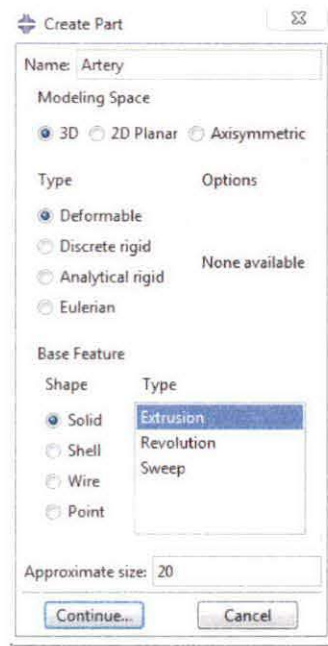
Figure C2. Create Part Window.

Click continue to enter the sketcher. Sketch a circle with an outside diameter of 5.45 mm and an inside diameter of 4.38 mm. Extrude the circles 32 mm to form a hollow cylinder. The hollow cylinder must be portioned to form the artery layers. A central axis must be made to partition the cylinder. Choose Create Datum Axis: Axis of Cylinder. Click the inside surface of the cylinder to create the datum axis.
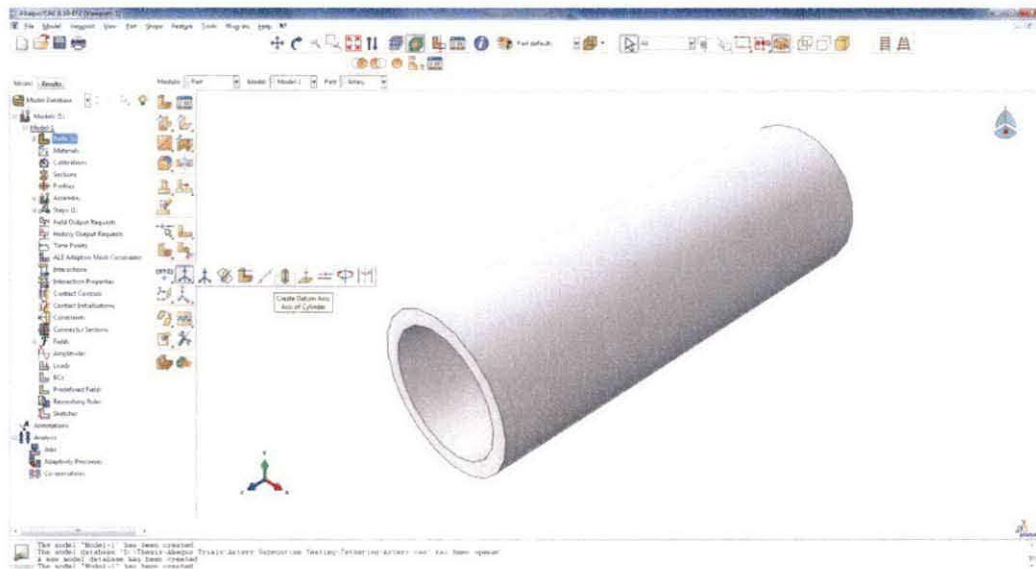
Figure C3. Create Datum Axis.

Once the axis is created, the cylinder can be partitioned to add the artery

layers. We will begin with the adventitia layer. Choose the Create Partition icon. A

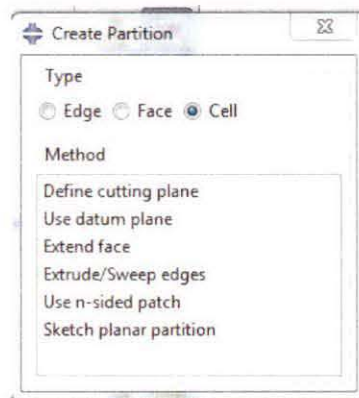partition will appear. Choose the Cell option.

Figure C4. Create Partition.

Choose Sketch Planar Partition. Click on the front face of the cylinder to

create a sketching surface. Next you will be asked to choose an edge. Choose the

outside edge of the cylinder. You will be then taken to the sketcher. Sketch a circle

with a diameter of 5.02 mm. After exiting the sketch, choose Extrude/Sweep Edges from the Create Partition window. Select the edge that you just sketched. Then choose Extrude Along Path. Choose the datum axis created earlier as the direction. Repeat these steps to create the media (diameter of 4.64 mm). The intima does not have to be partitioned, it will be automatically partitioned.

The artery must also be partitioned in order to add appropriate boundary conditions. Choose Define Cutting plane from the partition window. Select the entire artery as the cell. Choose normal to edge as the type. Select the outside edge of the artery. Small yellow circles will appear. Select these to create the partitions. Create partitions shown in Figure C5.
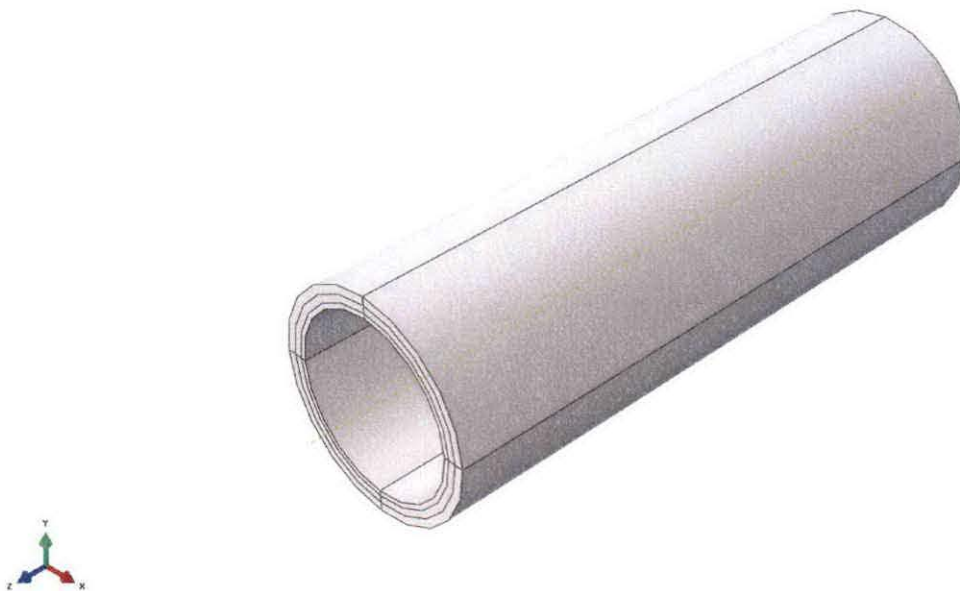

Figure C5. Partitioned Artery

The artery will now be meshed. Expand the part container on the left side bar. Double click mesh. Choose Seed → Part. Enter a global seed of 0.5. Choose Mesh → Controls. Select the entire artery. Change the technique to sweep and choose media axis. Choose Mesh → Part to mesh the artery. Choose Mesh → Element Type and deselect reduced integration.

Figure C6. Artery Mesh.

Materials are now created. Choose material from the side bar. A Create Material Window will appear. Enter adventitia as the name. Choose Mechanical → Elasticity → Hyperelastic. Change the strain energy potential to user. Select include compressibility. Repeat this for the media and adventitia.
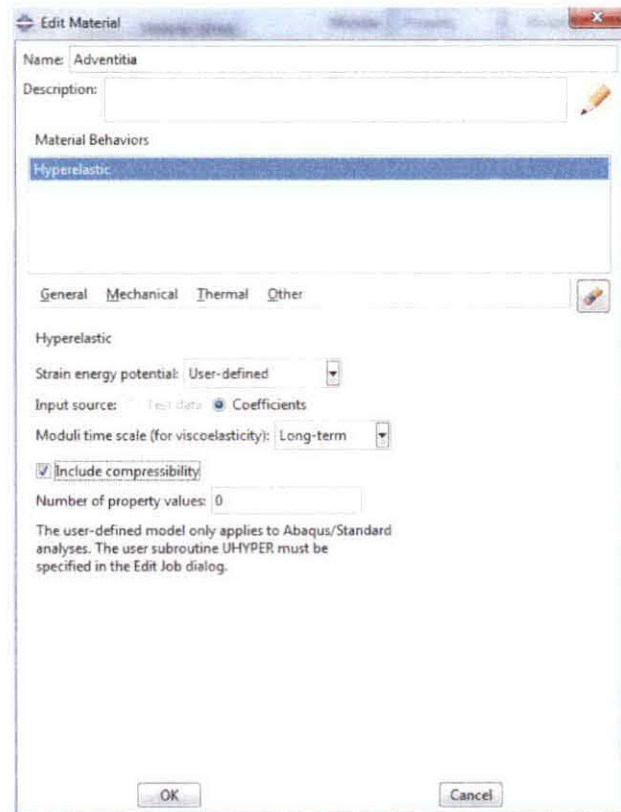
Figure C7. Create Material.

Choose Section from the side bar. Create a solid section named Adventitia.
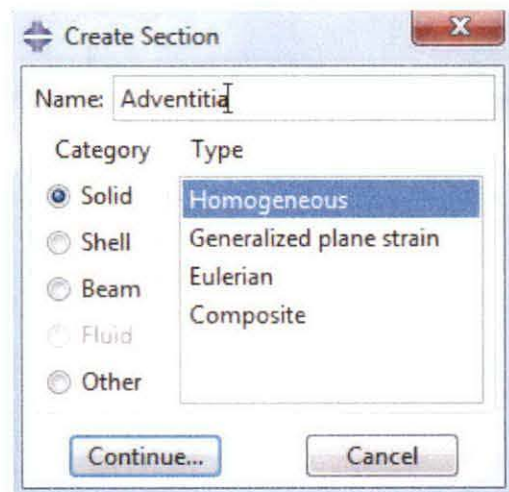

Figure C8. Create Section.

Click continue and change the material to adventitia. Repeat this for the media and intima. Choose Section Assignment from the expanded part container. Select the adventitia partions. Assign the adventitia section. Repeat for the media and intima.

Double click Assembly → Instances on the side bar. Add the artery to the assembly. Creating an assembly allows for boundary conditions and loads to be added to the model. Double click BCs on the side bar. Choose Displacement/Rotation. Choose the partition lines along the X axis. Constrain U2. Repeat for the Y axis (constrain U1).

Double Click Steps from the side bar. Create a static step named tethering. The NGLEOM option should be selected. Create boundary conditions on the front face of the artery (change the step to tethering). Set U3 to 8. Create a boundary condition of U3 equal -8 on the back face. This creates a displacement boundary condition that will lengthen the artery.

Create a new step named pulse. Select load. Choose pressure. Select the inside surfaces of the artery (lumen). Enter a value of 0.0002 for the magnitude.
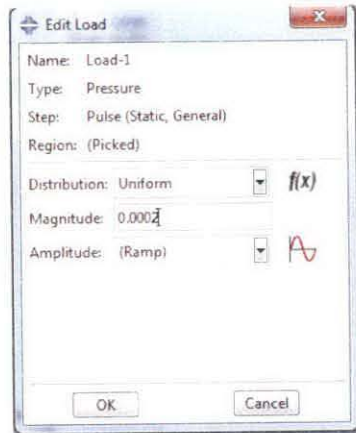
.

Figure C9. Pressure Creation.

Figure C10. Boundary Conditions and Pressure

Double click Jobs to create an analysis file. Under the general tab, find Select

User Subroutine. Browse to the uhyper subroutine. This shows the software where
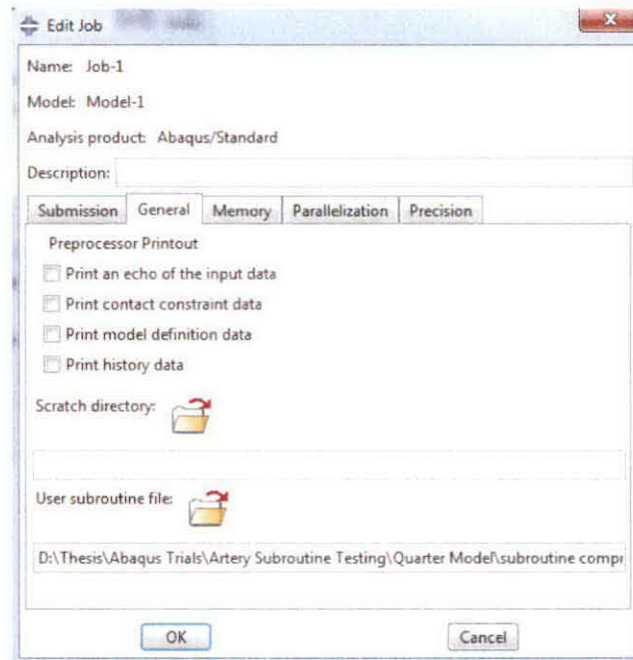
the material models are located.

Figure C11. Edit Job Window.

Right click on the job you just created and choose submit. Abaqus® will now perform the analysis. After the analysis completes, right click on the job again and choose results to view the results.